Comparison of intercept methods for correction of steady state relative permeability experiments for capillary end effects

Pål Ø. Andersen[1,2,*]

[1]Dep of Energy Resources, University of Stavanger, 4021 Stavanger, Norway

[2]The National IOR Centre of Norway, 4021 Stavanger Norway

[*]Corresponding author (pal.andersen@uis.no)

Abstract

Steady state relative permeability experiments are performed by co-injection of two fluids through core plug samples. The relative permeabilities can be calculated using Darcy's law from the stabilized pressure drop and saturation of the core if capillary end effects and transient effects are negligible. In most cases such conditions are difficult to obtain. Recent works have presented ways to extrapolate steady state pressure drop and average saturation measurements affected by capillary end effects collected at different rates to obtain correct relative permeabilities at correct saturations. Both the considered methods are based on linear extrapolations to determine intercepts. Gupta and Maloney (2016) derived their method intuitively and validated it with numerical and experimental data. Andersen (2021a) derived a method from fundamental assumptions and presented an intercept method in a different form where the saturation and relative permeabilities are found directly and uniquely from straight line intercepts. All system parameters, including saturation functions and injection conditions appear in the model.

In this work the two methods are compared. It is proven theoretically that Gupta and Maloney's method is correct in that it produces the correct saturation and pressure drops corrected for capillary end effects. Especially, a constant pressure drop was assumed and here proved to exist, as result of capillary end effects as addition to the Darcy law pressure drop with no end effects. Their method assumes a well-defined end effect region with length x_{CEE}, but this length can be defined almost arbitrarily. This choice has little impact on average saturation and pressure drop, however. They also assumed that for a defined end effect region, the average saturation there was constant and equal to the slope in their saturation plot. It is shown that if

the region is defined, the average saturation is indeed constant, but not given by the slope. The correct slope is predicted by the Andersen model.

We also comment on theoretical misinterpretations of the Gupta and Maloney method. A few works have correctly calculated that the pressure drop over the end effect region is independent of rate, but not accounted for that its length is rate dependent. We show that the combined pressure drop is equal to a constant plus the Darcy pressure drop over the full core.

Examples are presented to illustrate the model behaviors. Literature datasets are investigated showing that (a) apparently rate-dependent CO2-brine relative permeability end points can be explained by capillary end effects (b) the intercept methods can be applied to correct shale relative permeabilities.

Keywords: Capillary end effects; Intercept method; Steady state relative permeability experiment; Special core analysis; Capillary number

1 Introduction

Description of multiphase flow in porous media relies on two important parameters: the relative permeability and capillary pressure saturation functions. The former describes how much the effective permeability of a phase is reduced in the presence of another phase at a given saturation, while the latter expresses the difference in phase pressures at a given saturation. Both are measured in the laboratory using core plugs (McPhee et al. 2015). Our focus is on the measurement of relative permeabilities using the steady state technique: two phases are simultaneously injected into a core plug at specified rates and the average saturation and pressure drop are measured against time. When they have stabilized, it is often assumed that the saturation is uniformly distributed, and Darcy's law can then be applied to calculate the relative permeabilities.

It is however observed in many cases that the calculated relative permeabilities are affected by the measurement conditions (Osoba et al. 1951; Odeh et al. 1985; Henderson et al. 1998; Jeong et al. 2021), e.g. injection rate, core length, etc, (even for same fluid compositions, pressure and temperature). Relative permeabilities are expected to be independent of these properties and one can ask what values are correct or if they truly have such dependencies. The observations can in many cases be explained by the presence of capillary forces which cause accumulation of the more wetting phase near the outlet, where capillary pressure is zero (Leverett 1941; Richardson et al. 1952; Abeysinghe et al. 2012; Lenormand et al. 2017; Andersen 2020). The steady state saturation may then be shifted towards values with low

capillary pressure and the pressure drop increased compared to if capillary forces were negligible. Such effects are especially important to account for in the laboratory where length scales allow capillary forces to be significant. During forced imbibition (or drainage) capillary forces act as a resisting force to displacement, but during spontaneous imbibition (or drainage) capillarity is the driving force permitting oil and gas production (Bourbiaux and Kalaydjian 1990; Andersen et al. 2019; Andersen 2021b). The accumulation can be observed directly by means of in-situ imaging techniques such as computerized tomography and nuclear magnetic resonance (Hove et al. 1987; Wellington and Vinegar 1987; Cheng et al. 2015) but is expensive and not available in most laboratories. Chen and Wood (2001) measured in-situ saturation distributions and found that the relative permeabilities were rate independent when the saturations did not show signs of accumulation near the outlet. Zou et al. (2020) measured the saturation gradient to better estimate the capillary pressure.

A relative increase in advective forces over the capillary forces reduces the accumulation at the outlet and reduces the impact of capillary end effects. Several works have investigated how variations in system parameters, especially rate, affect steady state pressure drop and average saturation. Rapoport and Leas (1953) found that water breakthrough behavior in an oil-wet medium converged when the product of core length, rate and injected viscosity was sufficiently large and suggested this as a scaling parameter. Virnovsky et al. (1995) showed that the relative permeabilities and capillary pressure were analytically related to derivatives of phase pressure drop and saturation with respect to injected rate. Their analysis was tested experimentally using special inlet equipment (Virnovsky et al. 1998). Huang and Honarpour (1998) found implicit analytical relations for pressure drop and average saturation for single phase injection in strongly wetted media with Corey and Brooks (1964) saturation functions.

Based on measurements of pressure drop and fluid production against time, and even in-situ saturation profiles, numerical simulators can history match (invert) the data by assuming saturation function correlations and finding the correlation parameters that best reproduce the observations with forward simulations (Lenormand et al. 2017). Classic works have focused on finding one good (the best) match of the data, manually or automatically. A downside is that some parameters could be highly uncertain, the curves could be very uncertain on parts of the saturation interval, or a low number of tuning parameters could falsely indicate a narrow variation in predictions based on matching the available data. Recent works have put more focus into uncertainties or sensitivities and the range of parameterized correlations that give similar match of the data, and thus propagate the uncertainty of the data and its match to an ensemble (Valdez et al. 2020; Berg et al. 2021a,b). Although such techniques exist, an accurate

determination of the curves (with a range representing the experimental variation and less so the ability to estimate them) relies on obtaining data that can separate the contributions from advective and capillary forces, over as much of the saturation range as possible (Maas and Schulte 1997).

The main focus of this work is on so called intercept methods for correction of steady state relative permeability data, where the data in focus are stabilized (steady state) pressure drop and average saturation at a given injected fraction and rate. Gupta and Maloney (2016) suggested that there is a capillary end effect region with finite extent and fixed average saturation and that the presence of end effects adds a rate independent pressure drop to the pressure drop over the core resulting from Darcy's law without end effects. Measuring pressure drop and average saturation at different rates allowed determining this added pressure drop as the intercept of pressure drop against rate, thus allowing to correct the measured pressure data for end effects by subtracting this term. The corrected saturation was found as the intercept of a plot based on average saturation and assuming the ratio of pressure drop from end effects to corrected pressure drop was equivalent to the fractional length end effects covered the core. Most of their assumptions were not based on fundamental theory, but validated empirically and numerically. Further empirical support was provided in Reed and Maas (2018).

Andersen et al. (2017a) derived explicit solutions for water-flooding with end effects assuming simple saturation functions. Linear trends were obtained in average saturation and scaled pressure drop against inverse rate at high rates, providing correct end saturation and relative permeability. The model also gave analytical results at low rates and was used to determine entire capillary pressure and relative permeability functions from experimental data in Andersen et al. (2020). Andersen and Zhou (2020) obtained explicit solutions for co-injection type experiments, assuming linear saturation functions, again demonstrating linear trends at high rates with end effect corrected relative permeability points at the intercepts.

Moghaddam and Jamiolahmady (2019) derived that the pressure drop over the end effect region was constant (rate independent) and that the remaining pressure drop was given by the unaffected region of the core. They stated that this disproved Gupta and Maloney's assumption about pressure drop (being equal to unaffected pressure drop over the whole core plus a constant term). We will show that the findings actually are consistent as different pressure drop terms were compared in their work. They suggested that measurements at four rates at the same fraction were needed to determine four end effect region lengths, the end effect pressure drop, one corrected relative permeability end point and the corrected saturation, solving 8 equations. Then Darcy's law with the same corrected pressure gave the last relative permeability. Such a

comprehensive procedure is not necessary. As we will see, two rates are sufficient (mathematically) to calculate the corrected relative permeabilities and saturation.

Li et al. (2021) considered that relative permeabilities could be calculated from the unaffected zone in the core where end effects had not reached. If the length and pressure drop over this zone are known, Darcy's law gives correct relative permeabilities, corresponding with the constant saturation there. The (rate dependent) end effect length, unaffected relative permeability and pressure drop over the end effect zone were unknown, but could be determined with multiple tests. They found empirically from the data that the fractional length of the end effect region was proportional to, but not equal (as Gupta and Maloney assumed) the ratio of pressure drop over the end effect region to the corrected pressure drop and called it a stability factor. Nonetheless, their final method appears equivalent to Gupta and Maloneys method for obtained slope and intercept parameters. The main exception was perhaps using the slope through the pressure data to calculate relative permeability, rather than individual points along it. This is the same as averaging the estimates and does not invalidate Gupta and Maloney's method, as they claimed.

Andersen (2021a) derived general solutions for steady state flow of immiscible fluids with capillary end effects. It was shown that there is no well-defined end effect length since it takes infinite length to reach the unaffected saturation. However, when enough of the saturation profile is within the core, the impact on average saturation and pressure drop is as if there was a finite end effect length. At those conditions pressure drop and average saturation can both be scaled to one universal curve based on dimensionless numbers for all injection conditions. A more intuitive intercept method was derived: plotting average saturation and inverse effective relative permeability against inverse rate led to corrected saturation and corrected inverse relative permeability at the intercept (zero inverse rate). The effective relative permeability is simply based directly on the measured pressure drop. The method utilizes the pressure and saturation data independently and returns a single estimate for each based on all their data. Further, data from different cores and conditions could be plotted together and yield full relative permeability and capillary pressure curves. Further, given that only two straight lines can be obtained from pressure and saturation measurements in the high rate domain, 4 parameters (two slopes and two intercepts) are obtained from two rates at a given fraction. Performing more rates in the high rate domain will not provide more parameters, but can quantify the uncertainty. Low rates add more information since the point where linear trends stop and how the trends vary in the nonlinear domain (against inverse rate) provide useful information about the saturation functions, see examples of this in Andersen et al. (2017a, 2020).

Based on the general theory in Andersen (2021a), in this work we reexamine the method and assumptions made by Gupta and Maloney (2016) and the following works that have claimed inconsistencies in their model. Mainly we prove that their method is sound for finding corrected relative permeability and saturation and that some assumptions are incorrect (the existence of a well-defined end effect region length and that its fractional length is identical to a normalized pressure), but without impact on determining relative permeability points. Confusion related to rate-constant pressure drops from end effects being different is due to comparison of different parameters. Empirical relations are justified from theory.

The paper is structured as follows: In **Section 2** we present theory for steady state flow during co-injection of two phases including general equations for average saturation and pressure drop. Limits of these equations at high capillary numbers are derived in **Section 3** describing the Andersen (2021a) intercept method to correct relative permeabilities. These equations are compared to the intercept method by Gupta and Maloney (2016) and the claims by Moghaddam and Jamiolahmady (2019) and Li et al. (2021). Applications of the model are presented in **Section 4**. The paper is finalized with conclusions.

2 Theory

2.1 System geometry

In the steady state relative permeability experiment the system, illustrated in **Figure 1**, consists of a core with length L and we assume two fluids are injected at the inlet side $x = 0$. The fluids are produced at the outlet side $x = L$ where the capillary pressure is zero.

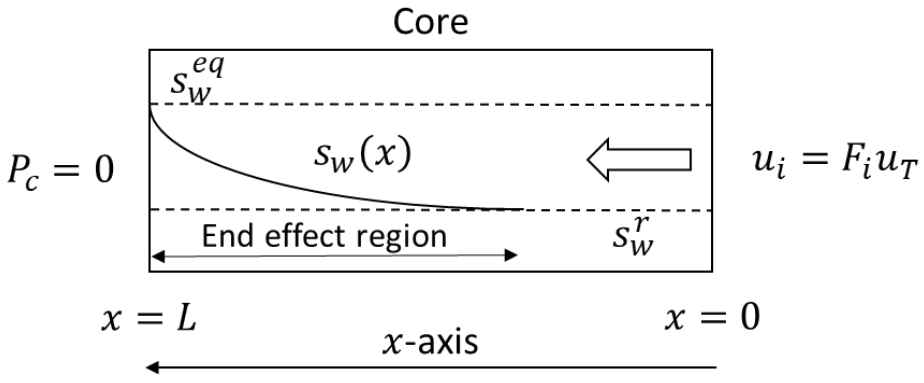

Figure 1 Model geometry (from Andersen 2021a) describing injection of two phases from the inlet at x=0 to the outlet at x=L where the capillary pressure is zero. s_w^r is the saturation with no end effects and s_w^{eq} is the saturation where capillary pressure is zero.

2.2 General model description

The mathematical description of 1D incompressible and immiscible flow of oil (o) and water (w) in a porous homogeneous medium is given by:

(1)	$\phi \partial_t s_i = -\partial_x u_i, \qquad (i = o, w)$
(2)	$u_i = -K\lambda_i \partial_x p_i, \qquad \lambda_i = \frac{k_{ri}}{\mu_i}, \qquad (i = o, w)$

where ϕ is porosity, s_i saturation, u_i Darcy velocity, K absolute permeability, λ_i mobility, k_{ri} relative permeability, μ_i viscosity and p_i pressure. Volume conservation and capillary pressure constraints state that:

(3)	$s_w + s_o = 1, \qquad p_o - p_w = P_c(s_w)$

The total Darcy velocity u_T is defined as:

(4)	$u_T = u_o + u_w = -K\lambda_T \partial_x p_w - K\lambda_o \partial_x P_c$

It follows from adding the transport equations in (1) that:

(5)	$\partial_x u_T = 0$

The water phase equation can then be expressed with variables u_T, s_w as:

(6)	$\phi \partial_t s_w = -\partial_x [u_T f_w + K\lambda_o f_w \partial_x P_c]$

where the water fractional flow function f_w is defined as:

(7)	$f_w = \frac{\lambda_w}{\lambda_w + \lambda_o}$

2.3 Boundary conditions

Water and oil are injected simultaneously at the inlet $x = 0$ with a water flow fraction F (the water fraction of the total injected flux) with a total Darcy flux u_T:

(8)	$u_w(x = 0) = u_T F$

The flux of a given phase is composed of both an advective and capillary component. From (6) we write this boundary condition as:

(9)	$u_w(x = 0) = [u_T f_w + K\lambda_o f_w \partial_x P_c]_{x=0} = u_T F$

The outlet boundary condition is described by a zero capillary pressure (Leverett 1941):

(10)	$P_c(x = L) = 0$

2.4 Steady State

At steady state we have no changes with time:

(11)	$\partial_t s_i = 0, \qquad \partial_t p_i = 0, \qquad (i = o, w)$

The phases are non-uniformly distributed due to the balance between advective and capillary forces. Water saturation and water pressure will be functions of spatial coordinate alone: $s_w(x)$ and $p_w(x)$. (6) can then be written as:

(12)	$$0 = d_x[u_T f_w + K(\lambda_o f_w d_x P_c)]$$

At steady state the fluxes are uniform, i.e., the same amount of water and oil passes through every cross section, however the saturations and velocities can differ. Setting the water flux uniformly equal to that at the inlet, see (9), gives:

(13)	$$u_w = u_T F = u_T f_w + K(\lambda_o f_w d_x P_c)$$

Using that $d_x P_c = P_c'(s_w) d_x s_w$, we can solve (13) with respect to the saturation gradient:

(14)	$$d_x s_w = \frac{u_T(F - f_w)}{K\lambda_o f_w P_c'} = \frac{u_T}{K}\frac{\left(\frac{F}{\lambda_w} - \frac{1-F}{\lambda_o}\right)}{P_c'}$$

The water saturation gradient is thus dependent on the two phase mobilities, the capillary pressure curve, the injected water flow fraction F and the injection flux u_T. We can further introduce the interstitial total velocity and dimensionless Leverett J-function (Dullien 2012):

(15)	$$u_T = \phi v_T, \qquad P_c = \sigma_{ow}\sqrt{\frac{\phi}{K}}J(s_w),$$

which results in:

(16)	$$d_x s_w = \frac{v_T\sqrt{\frac{\phi}{K}}}{\sigma_{ow}}\frac{\left(\frac{F}{\lambda_w} - \frac{1-F}{\lambda_o}\right)}{\frac{dJ}{ds_w}}$$

Let s_w^{eq} denote the saturation where capillary pressure is zero, $P_c(s_w^{eq}) = 0$. The above equation can be integrated starting from $s_w(x = L) = s_w^{eq}$. The pressure gradients of oil and water at steady state follow from (2) combined with (13):

(17)	$$d_x p_w = -\frac{u_T F}{K\lambda_w}, \qquad d_x p_o = -\frac{u_T(1-F)}{K\lambda_o},$$

The above corresponds to Darcy's law, where the water flux is constant equal to $u_T F$ and the mobilities vary according to the steady state saturation distribution found from (16). The equation (16) can be solved by separation into a space coordinate integral and a saturation integral:

(18)	$$\frac{v_T\sqrt{\frac{\phi}{K}}}{\sigma_{ow}}\int_x^{x'=L} dx' = \int_{s_w}^{s_w^{eq}} \frac{\frac{dJ}{ds_w}}{\frac{F}{\lambda_w} - \frac{1-F}{\lambda_o}} ds_w = \int_S^{S_{eq}} \frac{\frac{dJ}{dS}}{\frac{F}{\lambda_w} - \frac{1-F}{\lambda_o}} dS$$

Although the former is trivial, the latter in most cases requires numerical methods. We have introduced the normalized saturation S and related parameters as below:

(19)	$S = \frac{s_w - s_{wr}}{\Delta s_w}, \qquad ds_w = \Delta s_w dS, \qquad \Delta s_w = 1 - s_{or} - s_{wr}$
(20)	$\frac{dJ}{ds_w} = \frac{1}{\Delta s_w}\frac{dJ}{dS}, \qquad S_{eq} = \frac{s_w^{eq} - s_{wr}}{\Delta s_w}, \qquad S_r = \frac{s_w^{r} - s_{wr}}{\Delta s_w}$

It is also convenient to introduce the notations:

(21)	$Y = \frac{y}{L} = \frac{L - x}{L}, \qquad N_0 = \frac{v_T L\sqrt{\frac{\phi}{K}}\mu_m}{\sigma_{ow}}, \qquad \mu_m = (\mu_o\mu_w)^{0.5}$

Y is the relative distance from the outlet, N_0 is a capillary number containing known system parameters and μ_m is the mean viscosity. This leads to the solution form of interest:

(22)	$Y(S) = -\frac{1}{N_0}\int_{S_{eq}}^{S} \frac{\mu_m \frac{dJ}{dS}}{\frac{F}{\lambda_w} - \frac{1-F}{\lambda_o}} dS$

It follows directly that:

(23)	$\frac{dY}{dS} = -\frac{1}{N_0}\frac{\mu_m \frac{dJ}{dS}}{\frac{F}{\lambda_w} - \frac{1-F}{\lambda_o}} = -\frac{1}{N_0}\frac{\lambda_o f_w \mu_m \frac{dJ}{dS}}{F - f_w}$

which will be useful in upcoming calculations.

The average saturation follows from integrating the saturation along the core, but it can also be converted into a saturation integral evaluated from the scaled saturation S_{eq} at the outlet to the scaled saturation S_1 at the inlet $Y = 1$.

(24)	$\bar{S} = \int_{Y=0}^{1} S(Y)dY = \int_{S=S_{eq}}^{S_1} S\frac{dY}{dS}dS$

The latter saturation is found by solving $Y(S_1) = 1$, where $Y(S)$ is given by (22).

We define phase pressure drop as the inlet phase pressure minus the outlet phase pressure (zero for reference). First, define reference pressure drops without end effects:

(25)	$\Delta p_{i,ref} = \frac{L u_t \mu_i F_i}{K k_{rw}(S_r)} = \Delta p_{ref} = \frac{L u_t}{K \lambda_T(S_r)}$

As indicated, the pressure drop without end effects is equal for both phases. From Darcy's law, the pressure gradients of oil and water can be expressed in terms of the scaled distance from the outlet and the reference pressure:

(26)	$$\frac{dp_i}{dY} = \frac{Lu_T \mu_i F_i}{K k_{ri}\big(S(Y)\big)} = \Delta p_{ref} \frac{k_{ri}(S_\mathrm{r})}{k_{ri}\big(S(Y)\big)} > 0, \qquad (i = o, w)$$

The pressure drops including end effects are found by integration of the pressure gradients, expressed either as spatial integrals over the core or saturation integrals:

(27)	$$\Delta p_i = \Delta p_{ref} \int_{Y=0}^{1} \frac{k_{ri}(S_\mathrm{r})}{k_{ri}\big(S(Y)\big)} dY = \Delta p_{ref} \int_{S_{eq}}^{S_1} \frac{k_{ri}(S_\mathrm{r})}{k_{ri}(S)} \frac{dY}{dS}\, dS\,, \qquad (i = o, w)$$

Dividing (27) by this reference and applying the definition of $\frac{dY}{dS}$ from (23) we obtain:

(28)	$$\frac{\Delta p_i}{\Delta p_{ref}} = -\frac{1}{N_0} \frac{k_{ri}(S_r)\mu_m}{\mu_i} \int_{S_{eq}}^{S_1} \frac{1 - f_i}{F - f_w} \frac{dJ}{dS} dS > 0, \qquad (i = o, w)$$

We introduce an 'effective relative permeability' $\tilde{k}_{ri}$ based on the measured pressure drop and injection conditions by direct application of Darcy's law. This can be compared to the 'true' relative permeability without end effects $k_{ri}(S_\mathrm{r})$ which would be obtained if the pressure drop was Δp_{ref}.

(29)	$$k_{ri}(S_\mathrm{r}) = \frac{Lu_t \mu_i F_i}{K \Delta p_{ref}}, \qquad \tilde{k}_{ri} = \frac{Lu_t \mu_i F_i}{K \Delta p_i}, \qquad (i = o, w)$$

The ratio of pressure drops is then directly related to the ratio of relative permeability estimates:

(30)	$$\frac{\Delta p_i}{\Delta p_{ref}} = \frac{k_{ri}(S_\mathrm{r})}{\tilde{k}_{ri}}, \qquad (i = o, w)$$

This implies that the effective relative permeability approaches the true relative permeability when Δp_i approaches Δp_{ref}:

(31)	$$\tilde{k}_{ri} = k_{ri}(S_\mathrm{r}) \frac{\Delta p_{ref}}{\Delta p_i}, \qquad (i = o, w)$$

Under standard measurement conditions we only register the pressure drop of one phase, which is the less wetting phase at the injected fraction (oil can be less wetting than water at low water saturations and more wetting than water at high water saturations). This non-wetting phase pressure drop is the highest of the two (both phases have zero pressure at the outlet and nonwetting phase pressure is higher than wetting phase pressure) and implies that the effective relative permeability is always lower than the correct relative permeability.

(32)	$$\tilde{k}_{ri} = k_{ri}(S_\mathrm{r}) \frac{\Delta p_{ref}}{\Delta p_{nw}}, \qquad (i = o, w)$$

3 Intercept methods

3.1 Derivation of Gupta and Maloney method

Gupta and Maloney (2016) assumed a capillary end effect region with a length x_{CEE} less than the core length L and having a constant average saturation s_w^{CEE} (independent of rate). The remaining saturation profile had the remaining part of the core length, $L - x_{CEE}$ and a saturation corresponding to no end effects, s_w^r. The measured average saturation is then:

(33)	$$\bar{s}_w^{meas} = s_w^{CEE}\beta + s_w^r(1-\beta), \qquad \beta = \frac{x_{CEE}}{L}$$

As indicated, β is the fractional length of the core reached by the CEE region. They also assumed that the measured pressure drop is given by a constant contribution from the CEE region, called ΔP_I, plus an advective contribution from Darcy's law over the core:

(34)	$$\Delta p^{meas} = \Delta p_I + \frac{\mu_i L F_i u_t}{k_{ri}(s_w^r)K}, \qquad (i = o, w)$$

Note that the latter term corresponds to Δp_{ref} and that $k_{ri}(s_w^r)$ represents corrected relative permeabilities. Plotting measured pressure drop Δp^{meas} for different rates u_T should give a straight line with intercept Δp_I. After finding this value, any selected pressure drop can be corrected as:

(35)	$$\Delta p^{corr} = \Delta p^{meas} - \Delta p_I,$$

See **Figure 2a** for illustration. The relative permeabilities are then found from Darcy's law using the applied fraction and rate and the corrected pressure drop. Since the CEE length cannot be assessed easily, the fraction β was estimated by the fraction of CEE pressure to corrected pressure:

(36)	$$\beta = \frac{\Delta p_I}{\Delta p^{meas} - \Delta p_I} = \frac{\Delta p_I}{\Delta p_{ref}},$$

Dividing (33) by $(1-\beta)$, $\frac{\bar{s}_w^{meas}}{1-\beta}$ makes a straight line against $\frac{\beta}{1-\beta}$ with the corrected saturation s_w^r as intercept, also illustrated in **Figure 2b**:

(37)	$$\frac{\bar{s}_w^{meas}}{1-\beta} = s_w^{CEE}\frac{\beta}{1-\beta} + s_w^r$$

As this method relies on several assumptions, we will compare it to a more general method recently derived by Andersen (2021a).

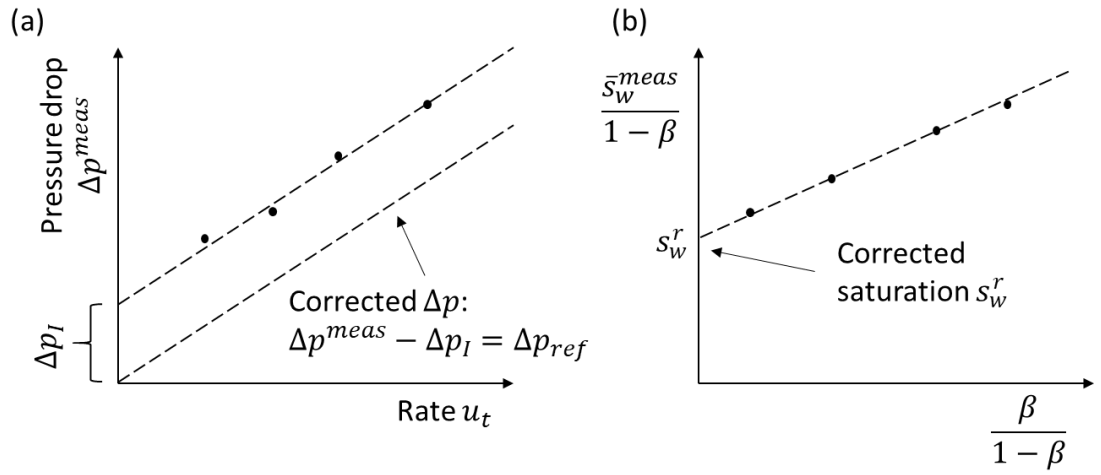

Figure 2 Illustration of Gupta and Maloney's intercept method. Correction of pressure drop (a) and saturation (b) for capillary end effects. The measured pressure drop is increased by a constant value due to end effects.

3.2 Derivation of Andersen method

Andersen (2021a) found that the position of the corrected saturation S_r extended to infinity for including all co-injection cases and either finite or infinite distance for single phase injection. However, we can consider a saturation S^* close to S_r which is located within the core at the fractional distance from the outlet denoted $Y^* = Y(S^*) < 1$, given by:

(38)	$$Y^* = -\frac{1}{N_0}\int_{S_{eq}}^{S^*} \frac{\mu_m f_w \lambda_o}{F - f_w}\frac{dJ}{dS}\,dS$$

The remainder of the core was assumed to have saturation S_r. Let $\bar{S}^*$ be the average saturation between the outlet and Y^* (in the end effect region) and $\bar{S}$ the average saturation of the core. We then have:

(39)	$$\bar{S} = \bar{S}^* Y^* + S_r(1 - Y^*),$$

The CEE average saturation $\bar{S}^*$ can be calculated as:

(40)	$$\bar{S}^* = \frac{1}{Y^*}\int_{Y=0}^{Y^*} S(Y)dY = \frac{1}{Y^*}\int_{S=S_{eq}}^{S^*} S\frac{dY}{dS}dS = \frac{\int_{S_{eq}}^{S^*} S\frac{\mu_m f_w \lambda_o}{F - f_w}\frac{dJ}{dS}\,dS}{\int_{S_{eq}}^{S^*} \frac{\mu_m f_w \lambda_o}{F - f_w}\frac{dJ}{dS}\,dS}$$

Inserting the expressions for $\bar{S}^*$ and Y^* from (40) and (38) into (39), the average saturation can now be expressed as:

(41)	$$\bar{S} = S_r + \frac{1}{N_0}\int_{S_{eq}}^{S^*} (S_r - S)\frac{\mu_m\left[f_w \lambda_o \frac{dJ}{dS}\right]}{F - f_w}\,dS,$$

We let $S^* \to S_r$ which causes the saturation integral to converge to a constant we call C_s:

(42)	$$C_s = \Delta s_w \int_{S=S_{eq}}^{S_r} (S_r - S) \frac{\mu_m f_w \lambda_o \frac{dJ}{dS}}{F - f_w} dS$$

This indicates that although some of the saturation profile extends beyond the core length, the average saturation is not much affected. Using unnormalized saturations we can write:

(43)	$$\bar{s}_w = s_w^r + \frac{C_s}{N_0} = s_w^r + \frac{C_s \sigma_{ow}}{L\sqrt{\frac{\phi}{K}}\mu_m} \frac{1}{v_T}$$

This states that average saturation plotted against inverse capillary number or inverse total velocity is linear and extrapolates to an intercept equal to the corrected saturation without end effects, see **Figure 3a**.

A similar analysis is performed for the pressure drop. We can evaluate the pressure drops in (27) as integrated from $Y = 0$ to Y^* and then adding the contribution from $Y = Y^*$ to 1 where the pressure gradient is constant as defined by the saturation S_r.

(44)	$$\Delta p_i = \Delta p_{ref} \int_{Y=0}^{1} \frac{k_{ri}(S_\mathrm{r})}{k_{ri}\big(S(Y)\big)} dY = \Delta p_{ref} \left[\int_{Y=0}^{Y^*} \frac{k_{ri}(S_\mathrm{r})}{k_{ri}\big(S(Y)\big)} dY + (1 - Y^*) \right], \quad (i = o, w)$$

The pressure drops over the end effect region can be evaluated as:

(45)	$$\Delta p_i^* = \Delta p_{ref} \int_{Y=0}^{Y^*} \frac{k_{ri}(S_\mathrm{r})}{k_{ri}\big(S(Y)\big)} dY = -\frac{\Delta p_{ref}}{N_0} \int_{S_{eq}}^{S^*} \frac{k_{ri}(S_\mathrm{r})}{k_{ri}\big(S(Y)\big)} \frac{\mu_m f_w \lambda_o \frac{dJ}{dS}}{F - f_w} dS$$

The remaining terms consist of Δp_{ref}, i.e. the pressure drop over the entire core if there were no end effects and minus this same pressure drop times the fractional length of the end effect region: $-\Delta p_{ref} Y^*$. This latter term is given as:

(46)	$$-\Delta p_{ref} Y^* = \frac{\Delta p_{ref}}{N_0} \int_{S_{eq}}^{S^*} \frac{\mu_m f_w \lambda_o}{F - f_w} \frac{dJ}{dS} dS$$

Both the pressure drop expressions Δp_i^* and $-\Delta p_{ref} Y^*$ consist of saturation integrals over the saturation range covered by the end effect and the factor $\frac{\Delta p_{ref}}{N_0}$ which can be evaluated as:

(47)	$$\frac{\Delta p_{ref}}{N_0} = \frac{\sigma_{ow}\sqrt{\frac{\phi}{K}}}{\mu_m \lambda_T(S_\mathrm{r})}$$

Both the pressure terms above are proportional to the magnitude of capillary forces, but independent of rate, meaning that the only rate-dependent term is Δp_{ref} which reflects the

pressure drop without end effects. Adding all the pressure terms and combining the saturation integrals allows to express the total pressure drops as:

(48)	$$\Delta p_i = \Delta p_{ref} + \frac{\Delta p_{ref}}{N_0}\frac{\mu_m}{\mu_i}\int_{S_{eq}}^{S^*}[k_{ri} - k_{ri}(S_\mathrm{r})]\frac{(1-f_i)}{F-f_w}\frac{dJ}{dS}dS\,, \qquad (i = o, w)$$

Note that the second term is just the sum of the two terms Δp_i^* and $-\Delta p_{ref} Y^*$ from (45) and (46) and thus constant. The combined saturation integrals are however not very sensitive to S^* and we let $S^* \to S_r$ to define the saturation integral constants C_w and C_o.

(49)	$$C_i = \int_{S=S_{eq}}^{S_r}[k_{ri} - k_{ri}(S_r)]\frac{(1-f_i)\frac{dJ}{dS}}{F-f_w}dS\,, \qquad (i = o, w)$$

The relation for pressure drop divided by the pressure drop without end effects is seen to be linear with the inverse capillary number (corrected for the phase viscosity) times the relevant saturation integral. Expanding the capillary number shows that the contribution from end effects is linear with inverse total velocity.

(50)	$$\frac{\Delta p_i}{\Delta p_{ref}} = 1 + \frac{1}{N_0\left(\frac{\mu_i}{\mu_m}\right)}C_i = 1 + C_i\frac{\sigma_{ow}}{L\sqrt{\frac{\phi}{K}}\mu_i}\frac{1}{v_T}, \qquad (i = o, w)$$

The measured pressure drop is that of the nonwetting phase at the injected fraction, given by:

(51)	$$\frac{\Delta p_{nw}}{\Delta p_{ref}} = 1 + \frac{1}{N_0\left(\frac{\mu_{nw}}{\mu_m}\right)}C_{nw} = 1 + C_{nw}\frac{\sigma_{ow}}{L\sqrt{\frac{\phi}{K}}\mu_{nw}}\frac{1}{v_T}$$

This can equivalently be expressed as:

(52)	$$\Delta p_{nw} = \Delta p_{ref} + \Delta p_I,$$
(53)	$$\Delta p_I = \frac{\Delta p_{ref} C_{nw}}{N_0\left(\frac{\mu_{nw}}{\mu_m}\right)} = C_{nw}\frac{\sigma_{ow}\sqrt{\frac{\phi}{K}}}{\lambda_T(S_\mathrm{r})\mu_{nw}}$$

where the first term Δp_{ref} is the pressure drop over the core without end effects and the second term Δp_I is the constant contribution from capillary end effects. Applying (51) in (32) the effective relative permeabilities can be expressed as:

(54)

$$\frac{1}{\tilde{k}_{ri}} = \frac{1}{k_{ri}(S_{\mathrm{r}})} + \left[\frac{C_{nw}}{k_{ri}(S_{\mathrm{r}})\left(\frac{\mu_{nw}}{\mu_m}\right)}\right]\frac{1}{N_0}$$

$$= \frac{1}{k_{ri}(S_{\mathrm{r}})} + \left[\frac{C_{nw}}{k_{ri}(S_{\mathrm{r}})}\frac{\sigma_{ow}}{L\sqrt{\frac{\phi}{K}}\mu_{nw}}\right]\frac{1}{v_T}, \quad (i = o, w)$$

stating that if we plot the inverse of effective relative permeability against inverse capillary number or inverse velocity, we get a straight line trend with intercept at the 'true' inverse relative permeability of each phase, see **Figure 3b**.

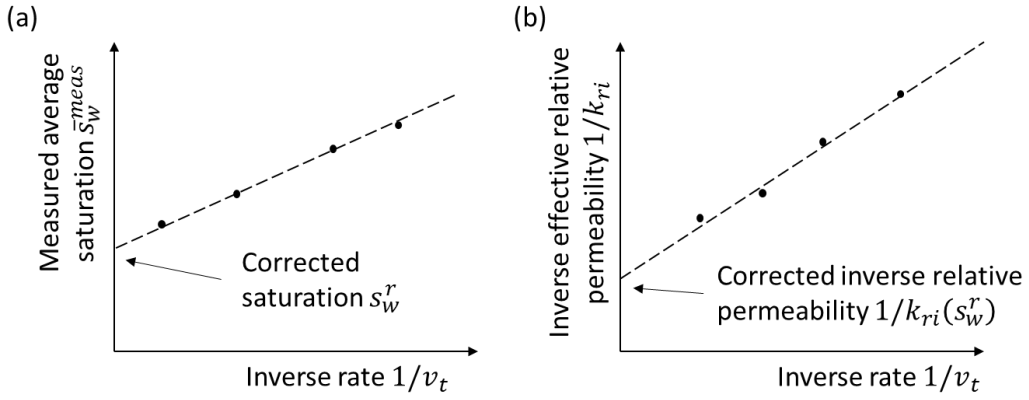

Figure 3 Illustration of Andersen's intercept method showing correction of saturation (a) and relative permeabilities (b) for capillary end effects. The effective relative permeabilities are reduced by end effects and increase towards the corrected value with higher rate. Inverse relative permeability is linear with inverse rate. Similarly, average saturation changes linearly with inverse rate (the slope depends on wettability).

3.3 Comparison of the methods

CEE region: As the saturation S_r does not have a finite distance, x_{CEE} is not defined other than subjectively. There will thus always be some end effect extending outside the core making the intercept method an approximation. However, the saturations closest to S_r have negligible impact on average saturation and pressure drop, making the linear relation between average saturation and fractional length, see (33) and (39), a better approximation the closer a fixed S^* is to S_r while being within the core.

Fixed CEE average saturation: Analytically, the profile does not change shape, but is only compressed or extended when the parameters in N_0 are varied while the saturation integral in (22) is held fixed. Again, assuming the main profile is within the core, we have shown in

(40) that the average saturation in the end effect region is a constant, as assumed by Gupta and Maloney.

Pressure plot and CEE term: (52) and (53) show that the measured pressure drop is given by the reference pressure drop over the core without end effects plus a term arising from capillary end effects which is independent of rate, confirming Gupta and Maloney's hypothesis in (34) and providing the actual value of this term.

Saturation plot: With the linear relation (33) being true, the linear relation (37) with s_w^r as intercept follows directly when β is defined in the same way as Y^* (a point with saturation S^* close but not identical to S_r).

Correspondence between Y^* and CEE pressure drop: The claim is that $Y^* = \frac{\Delta p_I}{\Delta p_{ref}}$. This claim is difficult to justify since depending on the choice of S^*, Y^* can take any value, while the term Δp_I (and the fraction $\frac{\Delta p_I}{\Delta p_{ref}}$) is constant. Taking the ratio of Y^* and $\frac{\Delta p_I}{\Delta p_{ref}}$ and using (38) and (52) we find that it is constant for a selected S^*:

(55)	$$C_* = \frac{Y^*}{\left(\frac{\Delta p_I}{\Delta p_{ref}}\right)} = -\frac{1}{C_{nw}}\left(\frac{\mu_{nw}}{\mu_m}\right)\int_{S_{eq}}^{S^*}\frac{\mu_m f_w \lambda_o}{F - f_w}\frac{dJ}{dS}dS$$

When (55) is applied in the expression for average water saturation (39) we obtain:

(56)	$$\bar{s}_w = \bar{s}_w^*\frac{\Delta p_I}{\Delta p_{ref}} + s_w^r\left(1 - \frac{\Delta p_I}{\Delta p_{ref}}\right) + [\bar{s}_w^* - s_w^r](C_* - 1)\frac{\Delta p_I}{\Delta p_{ref}}$$

This is written such that $\frac{\Delta p_I}{\Delta p_{ref}}$ appears in the first two terms in the same way as β does in (33).

Dividing (56) by $1 - \frac{\Delta p_I}{\Delta p_{ref}}$ we get a similar form as (37):

(57)	$$\frac{\bar{s}_w}{1 - \frac{\Delta p_I}{\Delta p_{ref}}} = \bar{s}_w^*\frac{\frac{\Delta p_I}{\Delta p_{ref}}}{1 - \frac{\Delta p_I}{\Delta p_{ref}}} + s_w^r + [\bar{s}_w^* - s_w^r](C_* - 1)\frac{\frac{\Delta p_I}{\Delta p_{ref}}}{1 - \frac{\Delta p_I}{\Delta p_{ref}}}$$

This is a linear equation of $\frac{\bar{s}_w}{1-\frac{\Delta p_I}{\Delta p_{ref}}}$ plotted against $\frac{\frac{\Delta p_I}{\Delta p_{ref}}}{1-\frac{\Delta p_I}{\Delta p_{ref}}}$, which has the corrected saturation s_w^r as intercept (when $\frac{\frac{\Delta p_I}{\Delta p_{ref}}}{1-\frac{\Delta p_I}{\Delta p_{ref}}}$ goes to zero). The presence of the third term demonstrates a different behavior when $\frac{\Delta p_I}{\Delta p_{ref}}$ is assumed to equal Y^*. This term is proportional to $\frac{\frac{\Delta p_I}{\Delta p_{ref}}}{1-\frac{\Delta p_I}{\Delta p_{ref}}}$ and means that the slope in the plot is not $\bar{s}_w^*$, but $\bar{s}_w^* + [\bar{s}_w^* - s_w^r](C_* - 1) = [\bar{s}_w^* - s_w^r]C_* + s_w^r$.

This is of less importance since we usually are not interested in estimating the CEE region average saturation $\bar{s}_w^*$. However, the dependence of S^* in the expression suggests that the slope might depend on the assumed S^*. Examining the involved expressions in the slope we find:

(58)	$\bar{s}_w^* = \Delta s_w \dfrac{\int_{S_{eq}}^{S^*} S \dfrac{\mu_m f_w \lambda_o \dfrac{dJ}{dS}}{F - f_w} dS}{\int_{S_{eq}}^{S^*} \dfrac{\mu_m f_w \lambda_o \dfrac{dJ}{dS}}{F - f_w} dS} + s_{wr}, \qquad C_* = -\dfrac{\left(\dfrac{\mu_{nw}}{\mu_m}\right)}{C_{nw}} \int_{S_{eq}}^{S^*} \dfrac{\mu_m f_w \lambda_o}{F - f_w} \dfrac{dJ}{dS} dS$
(59)	$[\bar{s}_w^* - s_w^r] C_* + s_w^r = \dfrac{\Delta s_w \left(\dfrac{\mu_{nw}}{\mu_m}\right)}{C_{nw}} \left[\int_{S_{eq}}^{S^*} (S_r - S) \dfrac{\mu_m f_w \lambda_o \dfrac{dJ}{dS}}{F - f_w} dS \right] + s_w^r$

We can let $S^* \to S_r$ in (59) and observe that the expression simplifies to:

(60)	$[\bar{s}_w^* - s_w^r] C_* + s_w^r = \dfrac{C_s}{C_{nw}} \left(\dfrac{\mu_{nw}}{\mu_m}\right) + s_w^r$

The saturation plot is then given by:

(61)	$\dfrac{\bar{s}_w}{1 - \dfrac{\Delta p_I}{\Delta p_{ref}}} = \left[\dfrac{C_s}{C_{nw}} \left(\dfrac{\mu_{nw}}{\mu_m}\right) + s_w^r\right] \dfrac{\dfrac{\Delta p_I}{\Delta p_{ref}}}{1 - \dfrac{\Delta p_I}{\Delta p_{ref}}} + s_w^r$

and does not depend on any subjective choice of S^*.

Application: It has been demonstrated theoretically that correct pressure drop and saturation will be obtained from the intercepts when using the intercept method by Gupta and Maloney. We argue however that the Andersen method is more intuitive and less sensitive to experimental errors. In Andersen's method, average saturation plotted against inverse rate directly provides the correct saturation, and inverse relative permeability plotted against inverse rate directly gives the correct (inverse) relative permeability. Gupta and Maloney's method applies separate plots of pressure drop vs rate and ratio of saturation to normalized pressure drop against other normalized pressure drop expressions which depend on regression parameters and measurements from the first analysis. Several corrected relative permeability estimates are obtained, without clear guidance on how to average them or select the best estimate. To avoid this ambiguity, we propose that neither of the data points should be applied, but instead an arbitrary point $(Q, \Delta p)$ on the regression line, as the line is based on all the data. With that modification, also the Gupta and Maloney method applies all the data to estimate one relative permeability. A minor disadvantage of their method in its original form is also that it depends on raw data (pressure drop) which in many cases is not reported, and must be combined with multiple other parameters (rate, permeability, viscosity, injected fraction, etc.) before

correction can be performed. The Andersen method only requires the interpreted relative permeability curves and the velocity (in any unit) they were measured at.

Uncertainty: The final estimated relative permeability point at a given flow fraction will be unique and correct when based on perfect data. However, when experimental data are applied to draw the line and intercept, noise and other sources of uncertainty (if the data are in the linear regime or have all reached steady state) can also lead to uncertainty in the estimated relative permeability point. This uncertainty can be quantified by the confidence interval of the intercept from the linear regression which can incorporate uncertainty in the data points if needed.

3.4 Comments on later works

Moghaddam and Jamiolahmady (2019) considered a strongly wetted medium with co-injection of incompressible gas and oil. They assumed an unaffected region and derived from steady state distributions similar to (40) that the average saturation in the end effect region should be constant, which is shown here for all wetting states. They also showed that there was a constant pressure drop over the end effect region, which corresponds to a less general version of (45). However, when they compared it to the pressure drop from the intercept method, which in fact is given by (53), they got a different answer and claimed the intercept method to be incorrect. However, the two parameters are both constant (with rate) and are mathematically different. Hence, seeing different values is no contradiction. In fact, the term Δp_I in (53) is more uniquely defined as it does not depend on the specific choice of S^*. Li et al. (2021) found empirically that the relation between Y^* and $\frac{\Delta p_I}{\Delta p_{ref}}$ was constant for a given injected flow fraction. That is proven theoretically in this work, see (55), where the actual ratio can be calculated from the input parameters. The factor however depends on the saturation S^* selected to define the extent of end effects.

4 Results and discussion

In the results we present interpretations of synthetical data and experimental data, where 'data' refer to steady state pressure drop and average saturation. The former is to show that the methods can reproduce data with an objectively correct answer (input relative permeability functions), the latter is to demonstrate that they can handle real measurements and evaluate consistency or differences in estimated relative permeabilities and related properties.

4.1 Interpretation of synthetical data

4.1.1 Input parameters

As input data for simulation we apply intrinsic parameters, relative permeabilities and scaled capillary pressure from Bourbiaux and Kalaydjian (1990) based on strongly water-wet Vosges sandstone. Their data were fitted to extended Corey relative permeability (Corey and Brooks 1964), where the exponents vary linearly with saturation, and Andersen et al. (2017b) capillary pressure correlation:

(62)	$k_{rw} = k_{rw}^{*}(S)^{n_w}, \qquad k_{rw} = k_{ro}^{*}(1-S)^{n_o}$
(63)	$n_w = n_{w1}S + n_{w2}(1-S), \qquad n_o = n_{o1}S + n_{o2}(1-S),$
(64)	$J(S) = \frac{J_1}{(1+k_1 S)^{n_1}} - \frac{J_2}{\left(1+k_2(1-S)\right)^{n_2}} + J_3$

S is normalized saturation. The saturation functions are plotted in **Figure 4** and the input parameters are listed in **Table 1**. To be precise, these inputs are applied on the examples in Sections 4.1.2, 4.1.3 and 4.1.4.

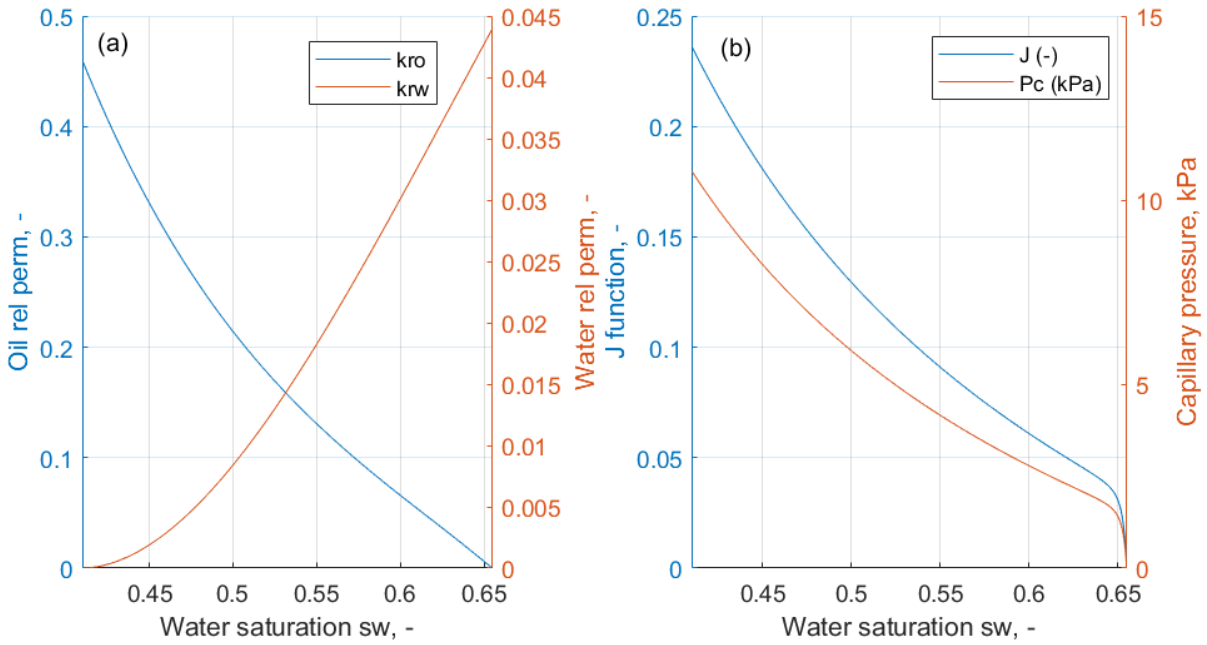

Figure 4 Input relative permeabilities (a) and capillary pressure (scaled and unscaled) (b) based on data from Bourbiaux and Kalaydjian (1990).

Table 1 Reference input parameters for simulations based on Bourbiaux and Kalaydjian (1990).

Constant parameters		Saturation function parameters					
K	137 mD	J_1	0.47291	k_{rw}^{*}	0.044	s_{wr}	0.41
ϕ	0.233	J_2	0.036769	k_{ro}^{*}	0.46	s_{or}	0.345

L	10 cm	J_3	-0.23646	n_{w1}	1.4	s_w^{eq}	0.655
σ_{ow}	0.035 N/m	k_1	1.16553	n_{w2}	1.8		
μ_w	1.2 cP	k_2	40	n_{o1}	1.1		
μ_o	1.5 cP	n_1	0.720448	n_{o2}	2.0		
		n_2	3				

4.1.2 Rate dependent relative permeabilities

As an initial illustration of the impact of capillary end effects we assume that the system described above is used to measure relative permeabilities at different flow fractions F and different total rates. Full curves are generated by spanning a large range of F from 0.01 to 0.99 in steps of 0.01 and keeping a fixed total rate. Rates from 1 PV/d to 1000 PV/d were considered. The results are shown in **Figure 5**. Although the same input relative permeabilities are used in each case, the effective relative permeability curves appear rate dependent. This is a result of end effects which add a higher pressure drop, reducing the calculated relative permeabilities at a given injected fraction. The saturations are shifted towards $s_w^{eq} = 0.655$ giving higher average saturations at a given injected fraction. At the highest rates (100 PV/d and up) the end effects are negligible: the relative permeabilities reach their highest values, are rate independent and the saturations span a greater interval as they have not been shifted towards s_w^{eq}. The calculated curves also equal the input curves.

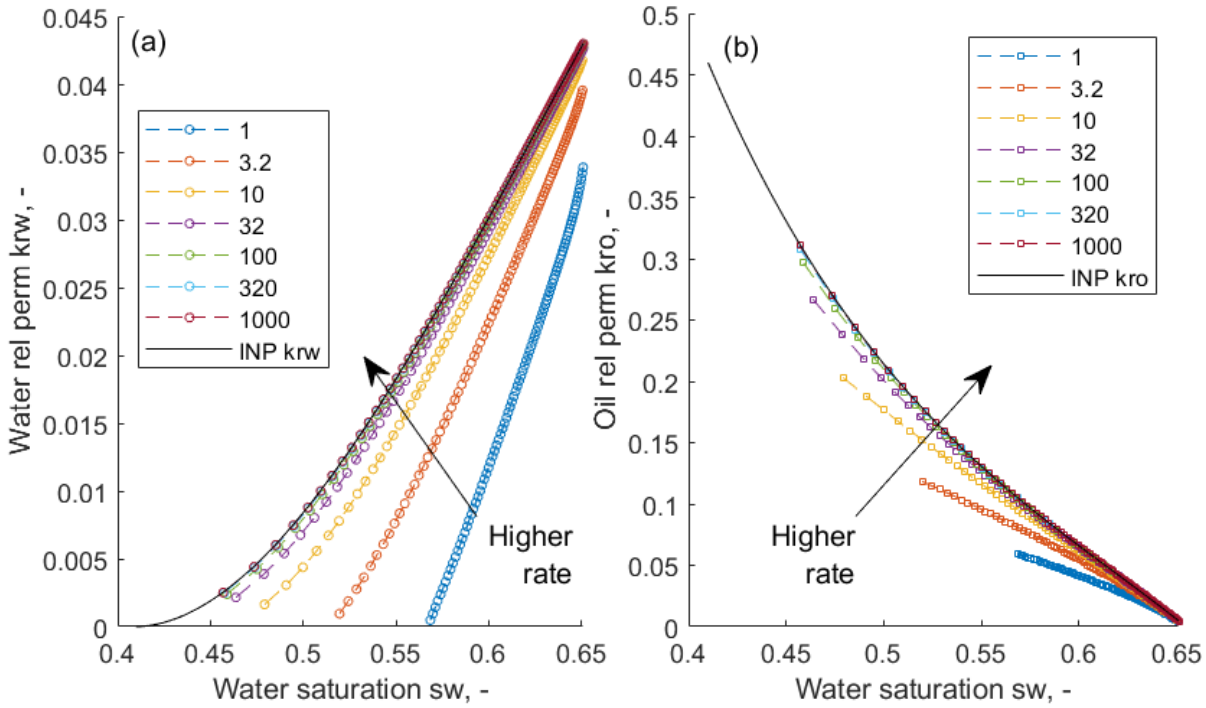

Figure 5 Effective relative permeabilities of water (a) and oil (b) based on injected fractions between 0.01 and 0.99. Each curve is based on a constant total rate in PV/d from 1 to 1000 as indicated.

4.1.3 Analytical prediction of linear behavior in high rate data

In practice it may not be possible to reach rates with negligible end effects, due to limitations in pump, pressure sensors, core integrity or significant deviation in flow conditions where the relative permeabilities can be expected to be unchanged, e.g. seen for capillary desaturation (Abeysinghe et al. 2012; Yeganeh et al. 2016). Then we need to apply the reliable measurements we can obtain to correct for end effects.

In the following example, the injected fraction $F = 0.05$ is applied with 6 total rates: 1, 2, 4, 8, 16 and 32 PV/d. According to the Andersen method, the average saturation and inverse (oil) relative permeability are plotted against inverse total rate in **Figure 6**. We have calculated the points according to the integrals (24) and (27) (as circles), which are valid for all steady states, and from the commercial simulator PRORES Sendra v2018.2.5 (as crosses) to confirm the numerical solution. At high rates (4 to 32 PV/d) the data fall on the straight lines predicted by the analytical solutions (43) and (54) and the lines have intercept at the correct saturation and correct inverse relative permeability (indicated as diamonds). Drawing a regression line through the high rate data with linear trend thus give correct results and will be demonstrated in the following sections.

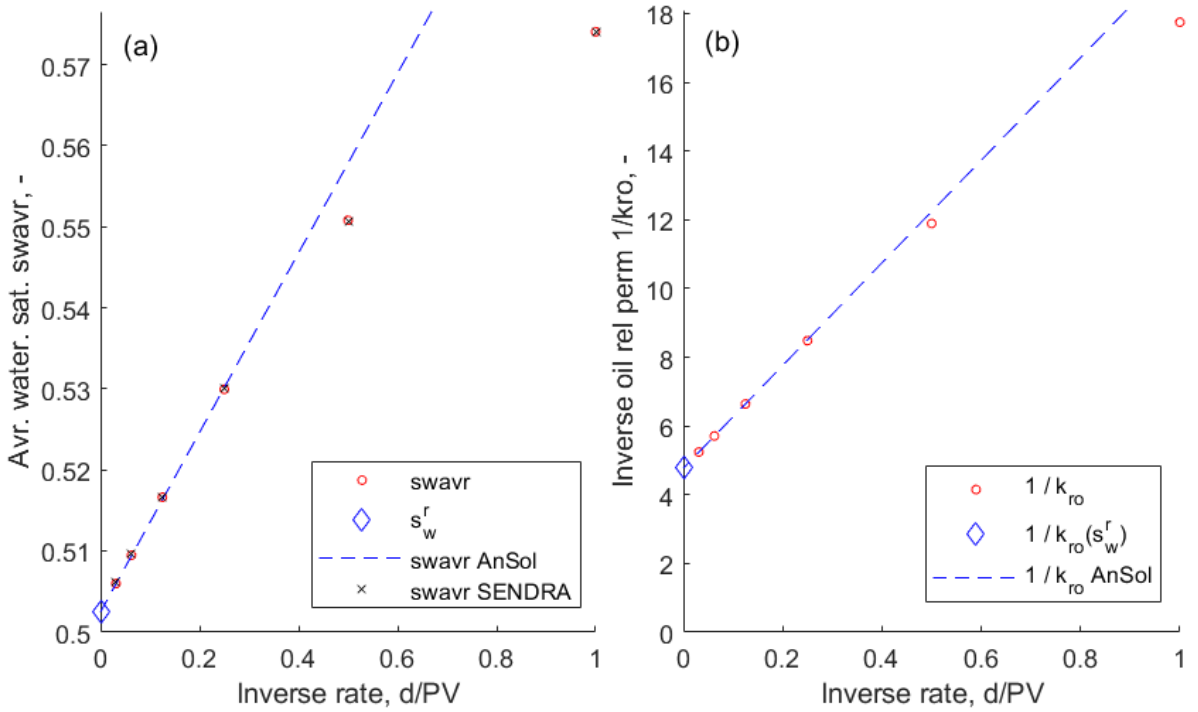

Figure 6 Plot of average saturation (a) and inverse relative permeability (b) against inverse total rate based on the reference input parameters at injected fraction $F = 0.05$. The lines are the analytical solutions for the high rate cases, extrapolated to lower rate.

We next plot pressure drop of non-wetting phase (oil) against total rate, and $\frac{s_{w,avr}}{1-\beta}$ against $\frac{\beta}{1-\beta}$ in **Figure 7**. In this plot we have defined β as $\beta = \frac{\Delta p_I}{\Delta p - \Delta p_I}$ and Δp_I is calculated from (53). Pressure drop calculated from SENDRA (crosses) agrees with our numerical calculations (circles). The analytical solution for pressure drop given by the sum of Δp_{ref} and Δp_I is a straight line that overlaps with the high rate points (4 to 32 PV/d) and matches the intercept Δp_I extrapolated to zero rate. Note that Δp_I is predicted correctly by (53). In the saturation plot the 4 high rate points fall on the predicted straight line (61) and the corrected saturation s_w^r is found at the intercept. The two low rate points fall on the negative side of the x-axis (as $\Delta p_I > 0.5\Delta p_{nw}$) and are not shown.

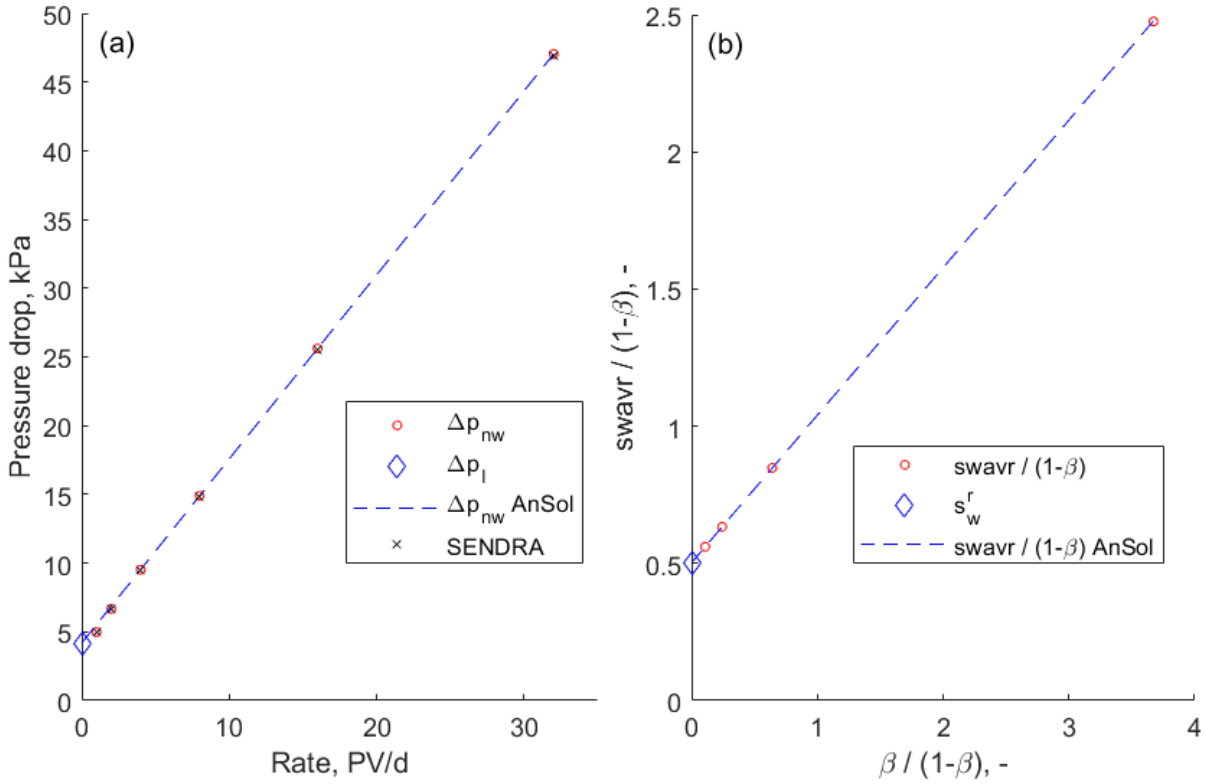

Figure 7 Plot of pressure drop against rate (a) and $\frac{s_{w,avr}}{1-\beta}$ against $\frac{\beta}{1-\beta}$ (b) demonstrating that the data form linear trends for the high rate points with the end effect pressure drop contribution Δp_I and corrected saturation s_w^r, respectively, at the intercepts. In (b) the two low rate points are on the negative x-axis and are not shown.

4.1.4 Non-unique quantities

Define the end effect length Y^* as where a saturation denoted $S^* \approx S_r$ is located, see (38). The two saturations cannot be identical since S_r is at infinite distance (Andersen 2021a), while S^* is not. Let S^* be defined as:

(65)	$S^* = S_r\varepsilon + S_{eq}(1-\varepsilon)$

for some ε close to, but less than 1. The (normalized) saturation S^* can be called a cut-off saturation because it is a practical way to define a finite end effect region. We did not need to make any assumptions on S^* in the previous section, as the parameters affecting the slope and intercept of the linear solutions (valid at high rates) are uniquely defined and depend on integrals covering the entire saturation interval between S_{eq} and S_r, while the general solutions for distributions and core average properties (valid at all conditions, but in integral form) depend on the distribution within the core. Our aim now is to see how the choice of cut-off saturation will affect properties associated with the end effect region (by this definition located at $0 <$

$Y < Y^*$). We consider the same example as before with $F = 0.05$ and apply the rate of 8 PV/d to demonstrate some impacts of the choice of S^*.

The saturation profile $s_w(Y)$ in **Figure 8a** is plotted with different S^* indicated with ε varying linearly from 0.99 to 0.9995. The closer S^* is selected to S_r, the longer the profile will be, as indicated by a larger Y^* and the added interval will have saturations more similar to S_r. Larger Y^* shifts the end effect average saturation towards S_r, see **Figure 8b**. This also demonstrates why the slope in Gupta and Maloney's saturation plot cannot equal the end effect average saturation. While the slope is unique, this average saturation is not. We also calculate the parameter $C_* = Y^* / (\frac{\Delta p_I}{\Delta p_{ref}})$ in **Figure 8c**. As we have demonstrated $\frac{\Delta p_I}{\Delta p_{ref}}$ is independent of S^*, while Y^* is not. The parameter C_* therefore changes proportionally with Y^*. Gupta and Maloney implicitly assumed C_* to be 1, although it is seen to differ, as it can take any value. Finally, in **Figure 8d** we see the pressure terms $-\Delta p_{ref} Y^*, \Delta p^*$, and their sum given either as $\Delta p^* - \Delta p_{ref} Y^*$ and as the constant Δp_I. The former two terms vary linearly in opposite ways with Y^*, while their sum is independent of Y^*.

We emphasize that if a specific choice of ε is made, the end effect cut-off saturation and end effect length Y^* will be properly defined, as will the end effect region average saturation $\bar{s}_w^*$ and the ratio $C_* = Y^* / (\frac{\Delta p_I}{\Delta p_{ref}})$. Once defined, the latter two are independent of rate and core length.

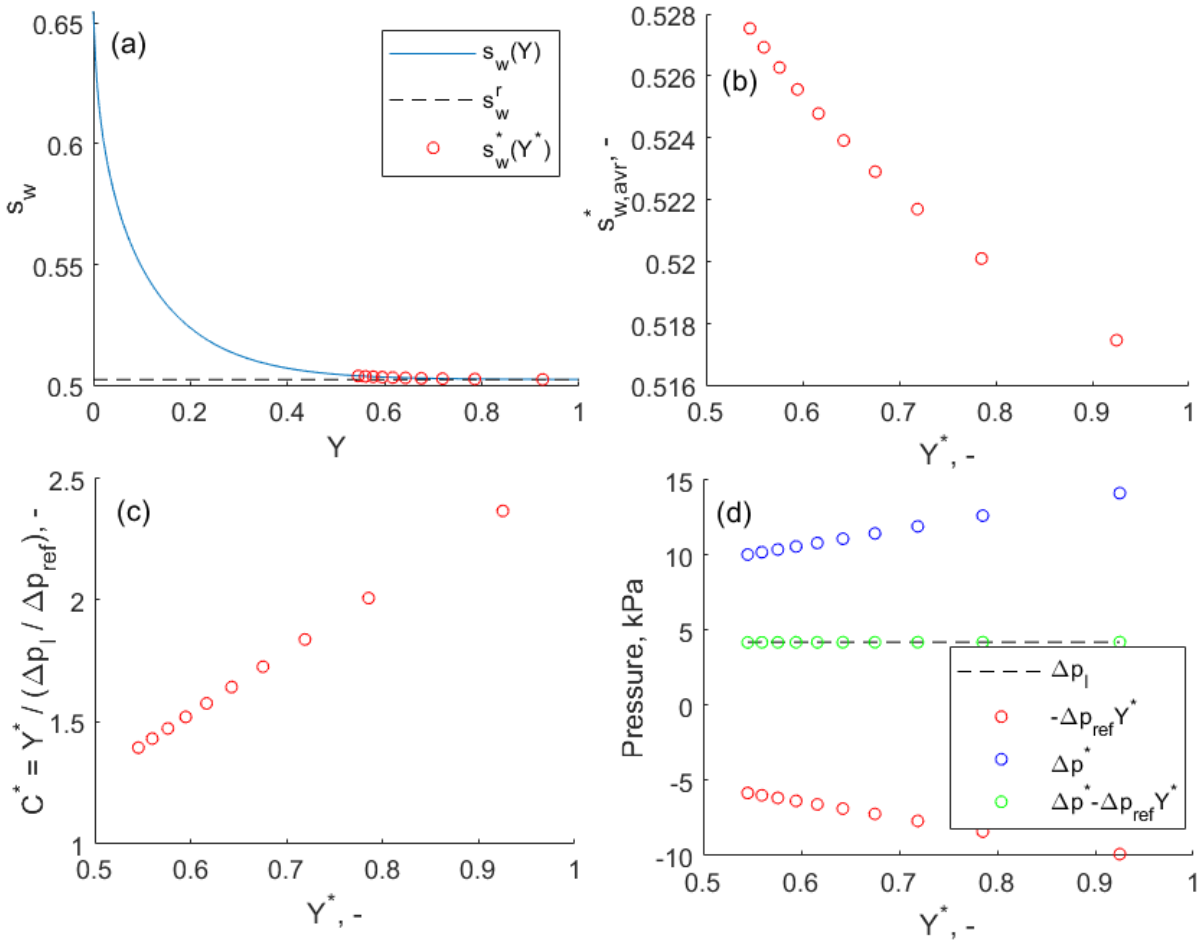

Figure 8 Simulation of the reference case with $F = 0.05$ and rate 8 PV/d. Saturation profile with end effect lengths Y^* marked at different cut-off saturations (a) and average saturation in the end effect region (b), the ratio between the end effect length and pressure ratio (c) and a comparison of the end effect related pressure drops (d) for different Y^*.

4.1.5 Moghaddam and Jamiolahmady synthetical data

Moghaddam and Jamiolahmady (2019) simulated steady state flow at two liquid-gas ratios (LGR) of 0.08 and 0.02, with known input saturation functions (capillary pressure and relative permeability) and hence, accurately known corrected relative permeabilities and saturations at the given injection conditions, called 'true'. The phases were assumed incompressible. They reported pressure drop and average saturation at four rates (for each LGR) where the end effect profile was within the core, i.e. conditions where the intercept methods are valid. Since they reported these values with four and three significant digits, respectively, that is also the accuracy we can expect in our estimates.

We first apply Andersen's method. In **Figure 9** average saturation (a) and calculated inverse effective relative permeabilities (b) are plotted against inverse total rate. The points align well on straight lines with very high R^2 (1.0000 for inverse relative permeabilities and

0.9994 for saturations). The difference between the saturation points and the line was less than 1.6e-4, and can be associated with the round-off of the fourth decimal. The corrected saturations (the intercepts) from the lines are 0.5602 (LGR=0.08) and 0.4497 (LGR=0.02). The corrected relative permeabilities from the lines are $k_{rg} = \frac{1}{6.449} = 0.1551$ (LGR=0.08) and $k_{rg} = \frac{1}{3.626} = 0.2758$ (LGR=0.02).

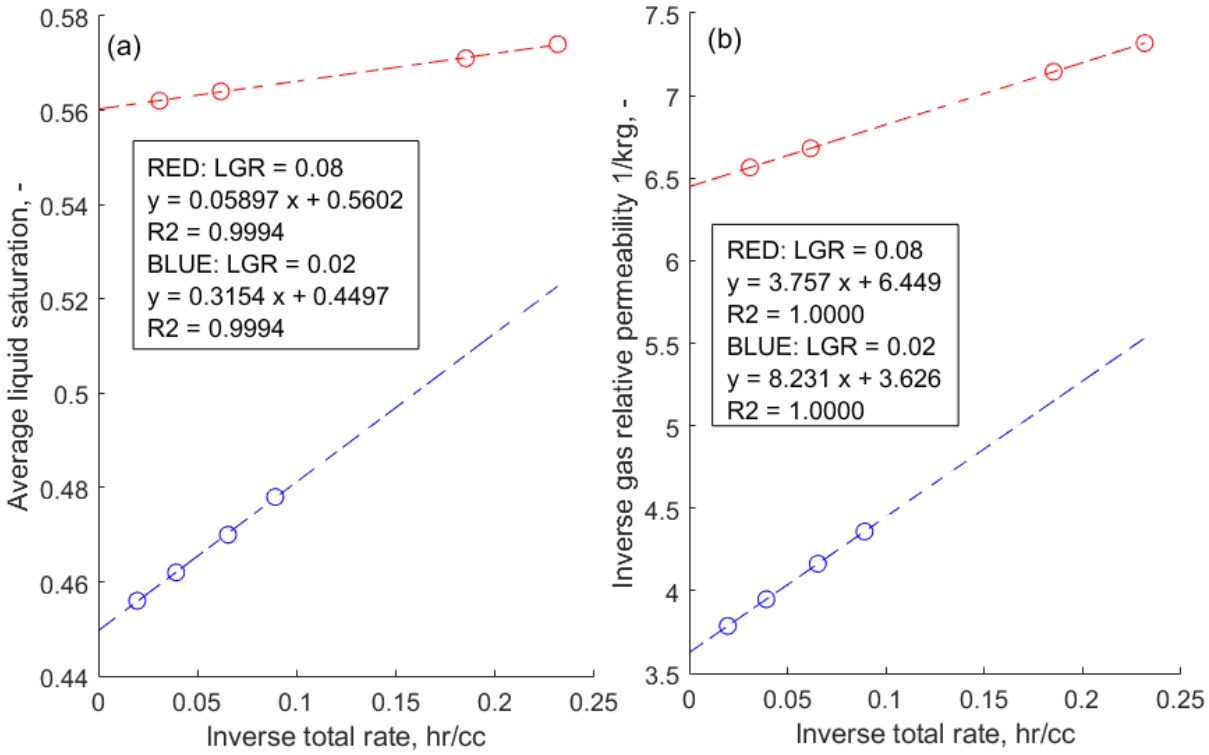

Figure 9 Plot of average saturation (a) and inverse relative permeability (b) against inverse total rate to determine corrected inverse relative permeability and corrected saturation at the intercepts of the regression lines. The data (points) are based on simulations from Moghaddam and Jamiolahmady (2019) and are expected to align on straight lines from Andersen's theory, with errors only resulting from round-off in reported data.

We also apply Gupta and Maloney's method by plotting pressure drop against rate in **Figure 10a** to find the end effect contribution to the pressure drop Δp_I at the intercept. Subtracting Δp_I from an arbitrary point on the regression line $\Delta p(Q)$ we find the corrected pressure drop and calculate relative permeability of gas. We calculate $\beta = \frac{\Delta p_I}{\Delta p - \Delta p_I}$ and plot $\frac{s_{avr}}{1-\beta}$ against $\frac{\beta}{1-\beta}$ in **Figure 10b** and draw a regression line to find corrected saturation at the intercept of this line. As we have proven Gupta and Maloney's method to be valid, we also observe that the points fall perfectly on the lines with R^2=1.0000 in the pressure and saturation plots.

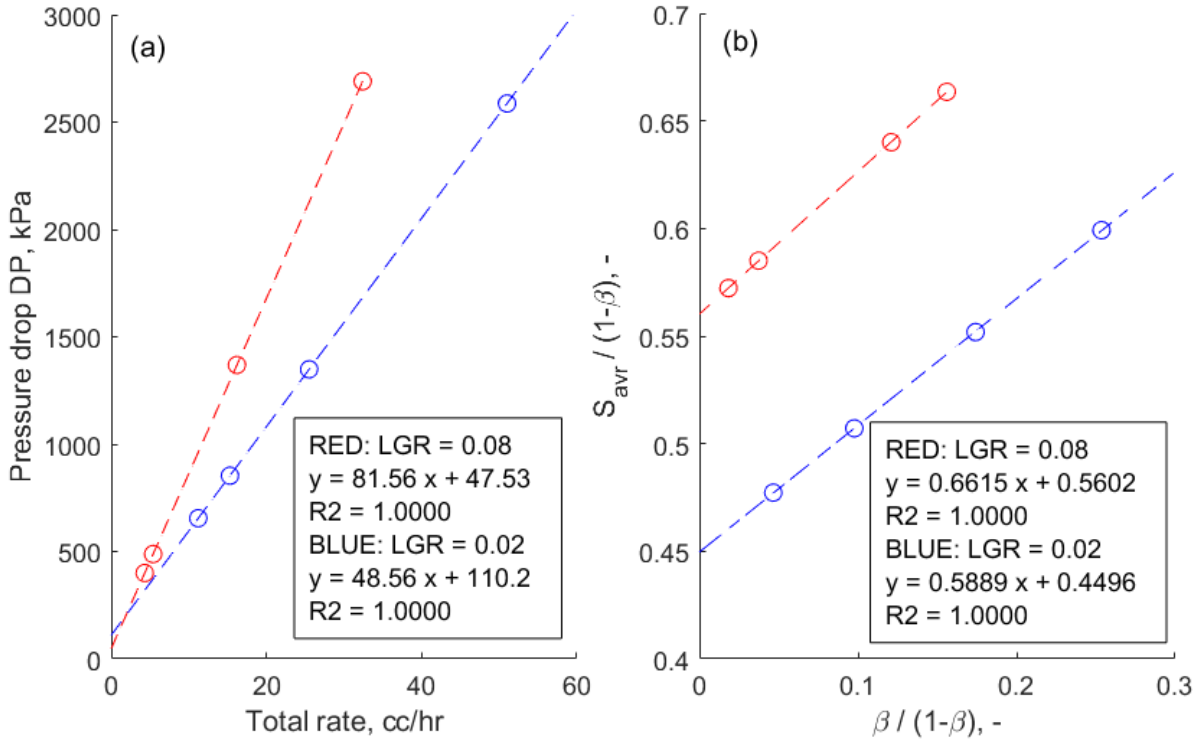

Figure 10 Plot of pressure drop against total rate (a) and $\frac{S_{avr}}{1-\beta}$ against $\frac{\beta}{1-\beta}$ (b) to determine end effect pressure drop and correct saturation, respectively, at the intercepts of the regression lines, according to Gupta and Maloney's method. The data (points) are based on simulations from Moghaddam and Jamiolahmady (2019).

The corrected relative permeability and saturation values obtained from the Andersen, Gupta and Maloney and Moghaddam and Jamiolahmady methods are summarized in **Table 2** together with the 'true' values. The three methods all provide estimates close to the true values. We note that Andersen and Gupta and Maloney's methods yield identical results to the fourth digit for all cases (although for LGR=0.02 there is a difference of 1 in the fourth digit for s_l). In particular k_{rg} is estimated to 0.1551 at LGR=0.08 and 0.2758 at LGR=0.02 with both these methods, which is virtually identical to the true values of 0.1550 and 0.2758 and interestingly better estimates than Moghaddam and Jamiolahmady's estimates of 0.1553 and 0.2826, where the latter has a relatively high error (2.5%). The three methods yielded saturations of 0.5602, 0.5602 and 0.5600 at LGR=0.08, virtually identical to the true value of 0.5600. For LGR=0.02, the saturation estimate from the three methods were 0.4497, 0.4496 and 0.4500 and have similar error ~ 0.001 compared to the true value of 0.4507. The slightly better saturation estimates by Moghaddam et al. are reasonable as they did not face round off errors in those data.

Note that Andersen and Gupta and Maloney's methods would have provided the same estimates using only two points (two rates) and performing two linear regressions. Moghaddam et al's method depends on four points (four rates) and simultaneously solving eight linear

equations for eight unknowns. It is also worth mentioning that although Moghaddam and Jamiolahmady pointed out that there exists an end effect pressure drop that is constant and not equal to the end effect pressure drop calculated by Gupta and Maloney's method, this is not inconsistent as both these constants exist. In the above examples we have illustrated that correct results are obtained.

Table 2 Comparison of corrected gas relative permeability and liquid saturation at two LGRs, based on the methods by Andersen (2021a), Gupta and Maloney (2016) and Moghaddam and Jamiolahmady (2019).

	LGR=0.08		LGR=0.02	
	s_l	k_{rg}	s_l	k_{rg}
Andersen	0.5602	0.1551	0.4497	0.2758
Gupta & Maloney	0.5602	0.1551	0.4496	0.2758
Moghaddam	0.5600	0.1553	0.4500	0.2826
True	0.5600	0.1550	0.4507	0.2758

4.2 Interpretation of experimental data

We present applications of the Andersen intercept method on three sets of experimental data. The interested reader can find applications of this method on two other sets of experimental data in Andersen (2021a).

4.2.1 Jeong et al. data: Rate-dependent CO_2 relative permeability end points

Jeong et al. (2021) measured steady state average water saturation and effective relative permeability of CO_2 at 14 different CO_2 single phase injection rates displacing water. They interpreted the trends as related to desaturation (reduction of residual saturation at higher capillary number), but did not check whether end effects could explain it. In fact, the capillary numbers they considered were in the same range as where water-oil did not have desaturation.

Their data are plotted as saturation and inverse relative permeability against inverse rate in **Figure 11**. With exception of the lowest rate data point, the data form straight lines with high coefficient of determination (~0.98) through the 13 high rate points, consistent with end effect behavior. The point that deviated from the straight line was below the line, in the sense of less change than if the linear trend continued. This is consistent with some of the end effect profile extending out of the core, with this part not affecting average saturation and pressure drop within the core, see Andersen (2021a). The core was strongly water-wet which means that the capillary forces retain water. End effects therefore support the observed reduced average water saturation with higher injection rate. The same was observed in Andersen et al. (2020) where

waterflooding to displace oil from an oil-wet core caused high oil saturations to be trapped at low rates. From the intercepts we find that the residual water saturation is $s_{wr} = 39.0\%$ and that the relative permeability of gas at that point is $k_{rg}(s_{wr}) = \frac{1}{2.063} = 0.485$.

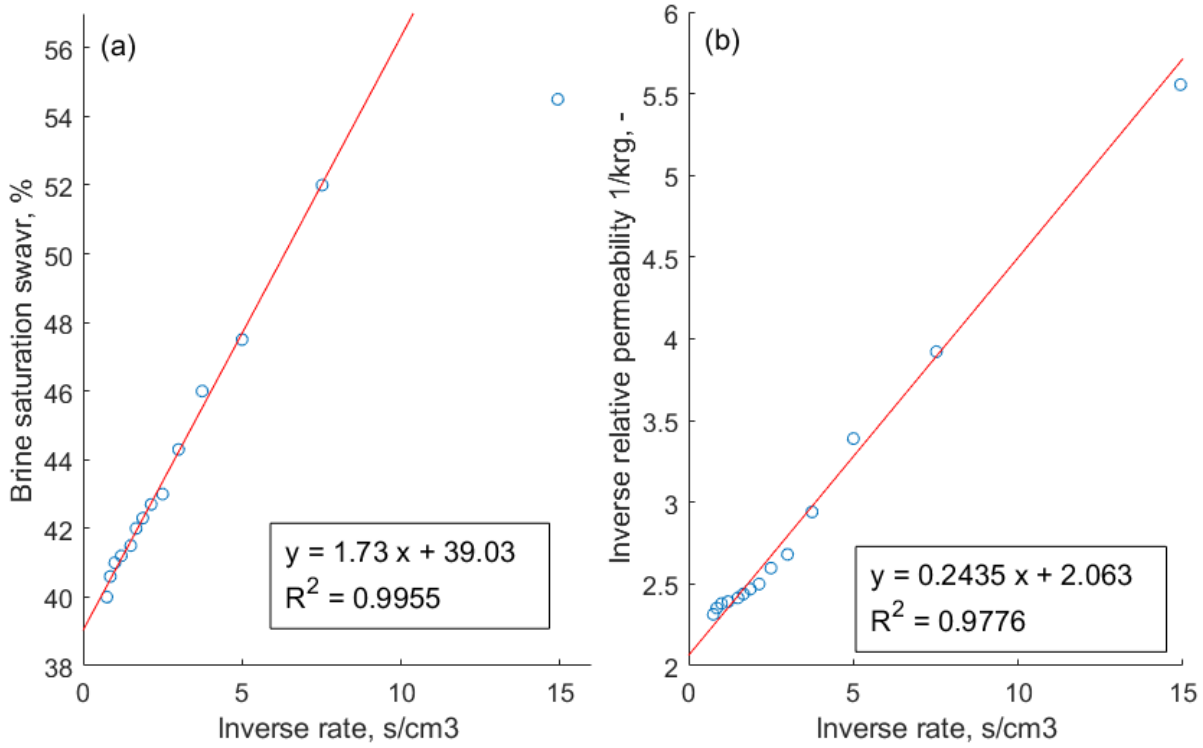

Figure 11 Plot of average saturation (a) and inverse gas relative permeability (b) against inverse rate during CO2 flooding to displace water. The experimental data (points) are from Jeong et al. (2021). Linear regression (red line) is performed through all points except the one with highest inverse rate which deviates from the linear trend, indicating the end effects have exceeded the core length.

4.2.2 Andersen et al. data: Waterflooding an oil-wet core

Andersen et al. (2020) waterflooded oil from a strongly oil-wet, high permeable Bentheimer sandstone core. This allowed capillary forces to be significant over a wide range of injection rates. Steady state pressure drop and saturations from stepwise increases in rate were used in that work to determine saturation functions over the entire saturation range. Here we demonstrate the Andersen intercept method on the data.

The average saturation and inverse effective water relative permeability are plotted against inverse rate in **Figure 12** with focus on the highest rates. As inverse rate goes to lower values, linear trends are identified and drawn through the four last points. From the intercepts the residual saturation is $s_{or} = 1 - 0.817 = 0.183$ and the relative permeability end point

$k_{rw}(1 - s_{or}) = \frac{1}{1.541} = 0.649$. Consistent with theory, the data at lower rates deviate from the lines in the direction of less impact.

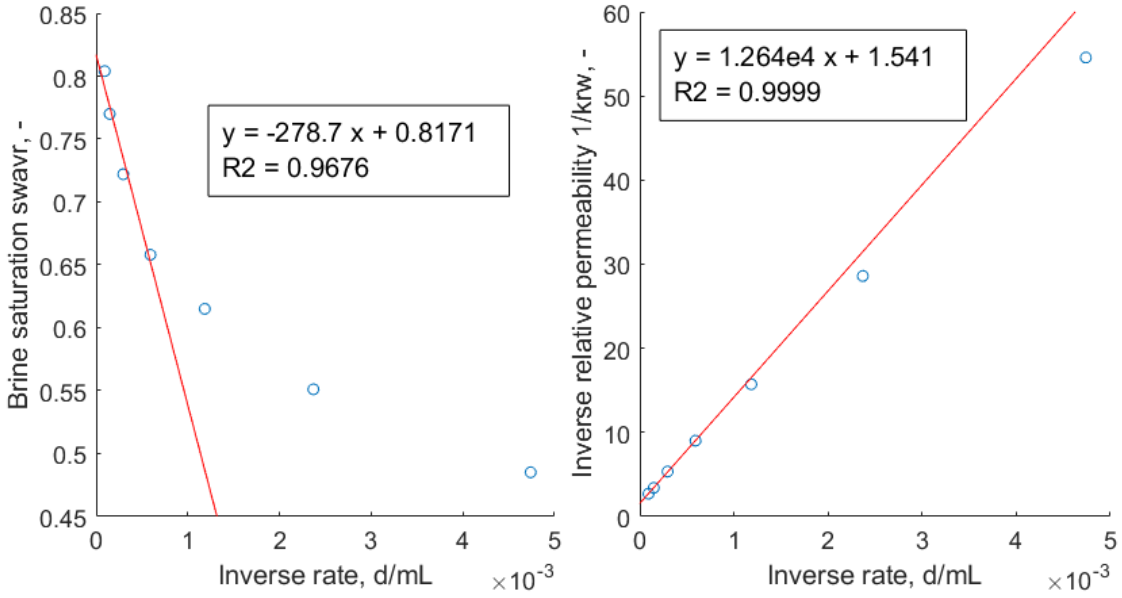

Figure 12 Plot of average saturation (a) and inverse water relative permeability (b) against inverse rate during water flooding to displace oil. The experimental data (points) are from Andersen et al. (2020). Linear regression (red line) is performed through the four points with lowest inverse rate. Points after that deviate from the linear trend, indicating the end effects have exceeded the core length.

4.2.3 Moghaddam and Jamiolahmady data: Gas-oil flow in shale

Moghaddam and Jamiolahmady (2019) injected oil and gas through a short shale core and reported relative permeability points at four total rates for four injection conditions: oil injection, gas injection, LGR=0.08 and LGR=0.25. For each injection condition we applied Andersen's method and plotted average saturation against inverse rate and inverse relative permeability against inverse rate and drew regression lines, see **Figure 13**. The LGR values were not necessary to interpret the data, but were applied for labeling. For the single phase injection conditions, the other phase has zero relative permeability and their data are hence not plotted (the inverse is infinite). The intercepts provided corrected saturation and corrected inverse relative permeabilities.

The saturations are shifted by end effects toward higher oil saturations for all conditions, indicative of a strongly oil-wet medium relative to gas. During gas injection for example, the end effects have great impact and modify the corrected saturation by as much as ~0.15. The oil injection saturations vary by just 0.02 from the intercept, but appear inconsistent in that lower oil saturations (0.82 vs 0.83) are obtained at higher oil rate which cannot be explained by

desaturation or end effects. A higher oil rate with zero gas rate should only increase the oil saturation. Assuming this to be experimental or reporting error, the average of these saturations 0.825 is assumed to be representative of the highest mobile oil saturation. There is no difference in the oil relative permeability end points (0.255) suggesting negligible influence of end effects during oil injection, consistent with strong oil-wetness.

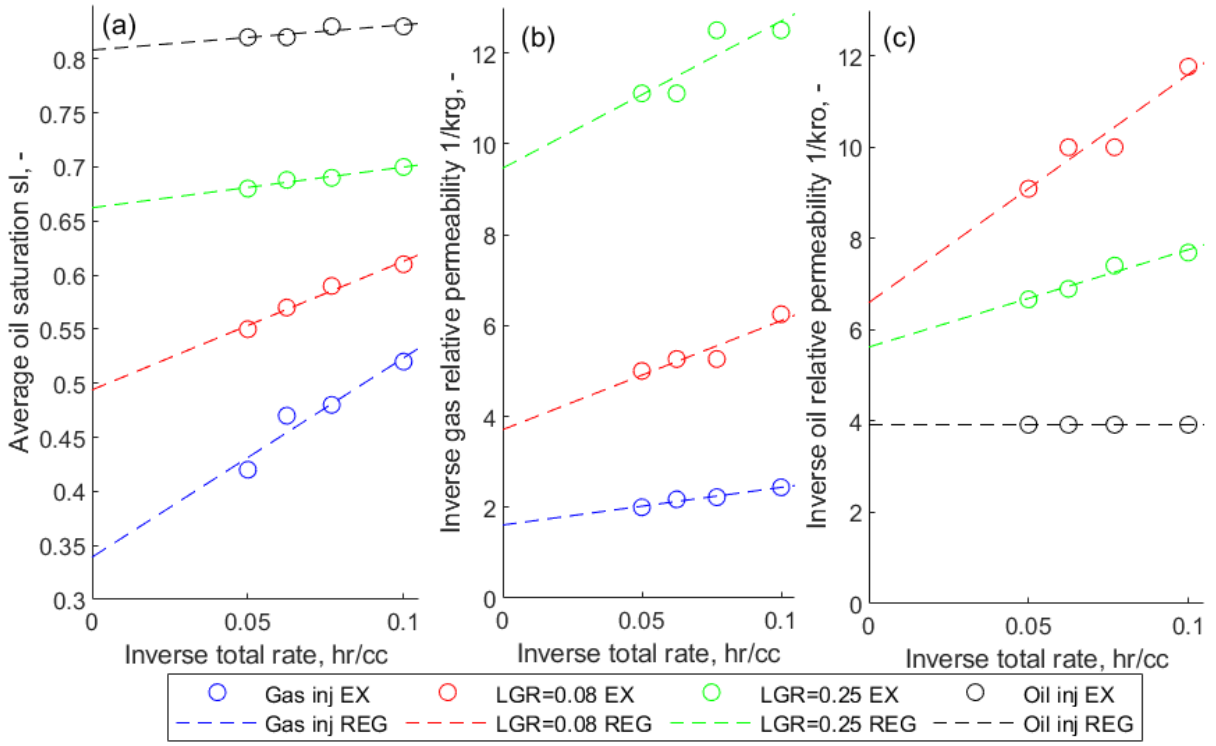

Figure 13 Illustration of Andersen's method to correct steady state experimental (EX) data. Plot of average oil saturation (a), inverse gas relative permeability (b) and inverse oil relative permeability (c) against inverse total rate. Corrected saturations and inverse relative permeabilities are found at the intercepts of the regression lines (REG). The data are from Moghaddam and Jamiolahmady (2019) based on 4 total rates and 4 injection conditions (identified by distinct colors).

Table 3 Corrected saturations and relative permeabilities after applying Andersen's method on experimental data from Moghaddam and Jamiolahmady (2019). *The oil injection saturation data appeared uninfluenced by end effects and their average was considered more representative than their intercept.

	Corrected oil saturation	Corrected gas relative permeability	Corrected oil relative permeability
Gas inj	0.339	0.621	0
LGR = 0.08	0.494	0.270	0.152
LGR = 0.25	0.662	0.106	0.178
Oil inj	0.825*	0	0.255

The corrected results are summarized in **Table 3**. The corrected points are also plotted together with the curves measured at different rates in **Figure 14**. At a given injection condition the nonzero relative permeabilities are increased after correction for end effects. The corrected saturations span a greater saturation interval, as they are no longer shifted towards the saturation where capillary pressure is zero (in this case 0.825).

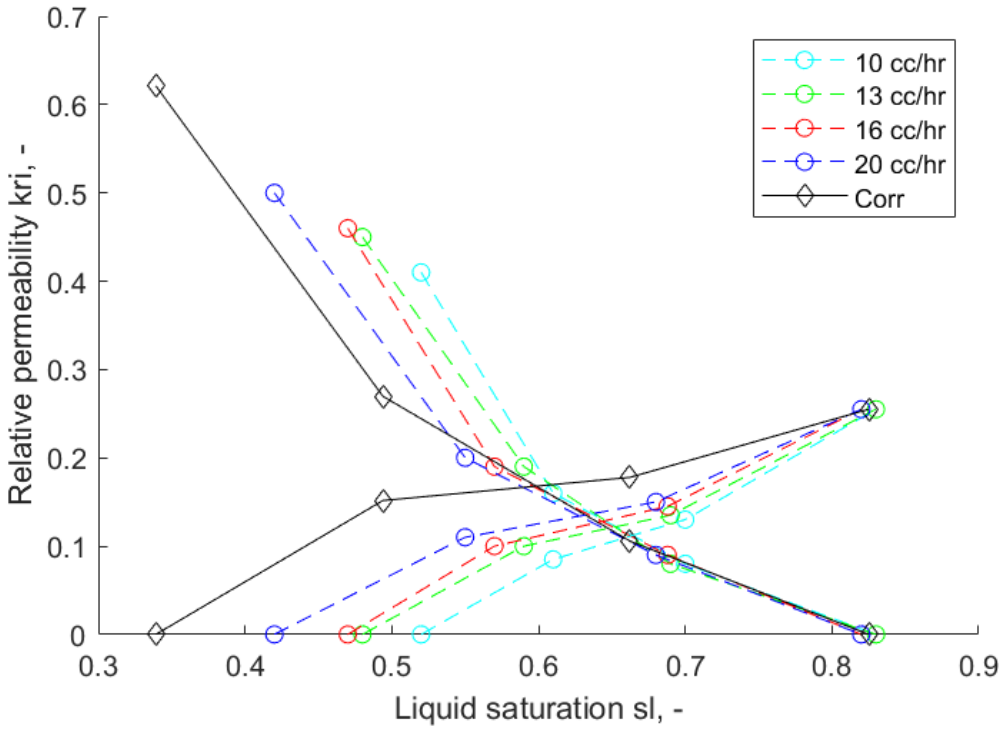

Figure 14 Oil and gas relative permeability points measured at different total rates (dashed lines) by Moghaddam and Jamiolahmady (2019) and the corrected curves (full lines) based on the Andersen method.

5 Conclusions

General equations have been derived for steady state flow of two immiscible phases through a core subject to capillary end effects. The theoretically derived intercept method by Andersen (2021a) was compared with the intercept method by Gupta and Maloney (2016) which was based on less clear assumptions. Andersen's method states how all the system parameters are related to experimental observations. In its simplest form it states that to obtain corrected steady state data: plot average saturation and inverse relative permeability against inverse total rate at a given injected fraction and interpolate a straight line through the high rate data that are linear to read corrected saturation and corrected inverse relative permeability at the intercepts. The following was concluded:

- Gupta and Maloney's intercept method could be derived from the general solution. The slopes and intercepts were predicted and are not subjective to how the end effect region is defined. Specifically, it was proven that:
    - Drawing pressure drop against total rate (for a fixed injected fraction) gives an intercept which is a constant term Δp_I from capillary end effects. The remaining pressure drop is the pressure drop from Darcy's law without end effects Δp_{ref} which is proportional to rate. Δp_{ref} contains correct relative permeability values from Darcy's law.
    - It was proven that $\Delta p_I / \Delta p_{ref}$ is not equal, but proportional to the fractional length of the end effect region (relative to the core). That is also a formal proof of the empirical observation by Li et al. (2021). Gupta and Maloney's saturation plot based on $\Delta p_I / \Delta p_{ref}$ does provide the end effect corrected saturation s_w^r at the intercept, but the slope in this plot does not equal the average saturation in the end effect region.
- Several properties of the end effect region are subjective. The unaffected saturation does not have a finite distance and a cut-off saturation must be defined. This choice affects the length, average saturation and pressure drop over the end effect region (which is not the same as the intercept Δp_I). Using such non-unique quantities as matching parameters to determine corrected relative permeability and corrected saturation is unnecessary and requires justification.
- Literature data showing apparently rate dependent relative permeabilities in a CO2-brine system could be explained by capillary end effects.

An advantage of the intercept method is explaining how measurements are related to physics in the system (e.g., saturation increase or decrease with rate implies wettability) and providing accurate relative permeability points based only on the relevant data. Since the results are analytical, they also inform about data quality / consistency and whether the end effect is within the core. With full numerical simulation, the user may manually 'guess' what to vary and how to match the data, which is challenging when the entire forecast is affected. Alternatively, an automated match can be less transparent regarding which data features resulted in the match and how accurate, unique and dependent the parameters are. The intercept method quickly provides reliable relative permeability points and should be supplementary to numerical history matching for assessing consistency.

Acknowledgments

The author acknowledges the Research Council of Norway and the industry partners, ConocoPhillips Skandinavia AS, Aker BP ASA, Vår Energi AS, Equinor ASA, Neptune Energy Norge AS, Lundin Norway AS, Halliburton AS, Schlumberger Norge AS, and Wintershall DEA, of The National IOR Centre of Norway for support.

References

1. Abeysinghe, K. P., Fjelde, I., & Lohne, A. (2012, April). Dependency of remaining oil saturation on wettability and capillary number. In *SPE Saudi Arabia Section Technical Symposium and Exhibition*. OnePetro.
2. Andersen, P. Ø., Standnes, D. C., & Skjæveland, S. M. (2017a). Waterflooding oil-saturated core samples-Analytical solutions for steady-state capillary end effects and correction of residual saturation. *Journal of Petroleum Science and Engineering*, *157*, 364-379.
3. Andersen, P. Ø., Skjæveland, S. M., & Standnes, D. C. (2017b, November). A novel bounded capillary pressure correlation with application to both mixed and strongly wetted porous media. In *Abu Dhabi International Petroleum Exhibition & Conference*. Society of Petroleum Engineers.
4. Andersen, P. Ø., Brattekås, B., Nødland, O., Lohne, A., Føyen, T. L., & Fernø, M. A. (2019). Darcy-Scale simulation of Boundary-Condition effects during Capillary-Dominated flow in high-permeability systems. *SPE Reservoir Evaluation & Engineering*, *22*(02), 673-691.
5. Andersen, P. Ø. (2020). Capillary Pressure Effects on Estimating the Enhanced-Oil-Recovery Potential During Low-Salinity and Smart Waterflooding. *SPE Journal*, *25*(01), 481-496.
6. Andersen, P. Ø., Walrond, K., Nainggolan, C. K., Pulido, E. Y., & Askarinezhad, R. (2020). Simulation interpretation of capillary pressure and relative permeability from laboratory waterflooding experiments in preferentially oil-wet porous media. *SPE Reservoir Evaluation & Engineering*, *23*(01), 230-246.
7. Andersen, P. Ø., & Zhou, Y. (2020). Steady state relative permeability experiments with capillary end effects: analytical solutions including derivation of the intercept method. *Journal of Petroleum Science and Engineering*, *192*.
8. Andersen, P. Ø. (2021a). Analytical modeling and correction of steady state relative permeability experiments with capillary end effects – An improved intercept method,

scaling and general capillary numbers. *Oil & Gas Science and Technology - Rev. IFP Energies nouvelles*, *76*(61).

9. Andersen, P. Ø. (2021b). Early and late time analytical solutions for co-current spontaneous imbibition and generalized scaling. *SPE Journal*, *26*(1), 220-240.
10. Berg, S., Unsal, E., & Dijk, H. (2021). Non-uniqueness and uncertainty quantification of relative permeability measurements by inverse modelling. *Computers and Geotechnics*, *132*, 103964.
11. Berg, S., Unsal, E., & Dijk, H. (2021). Sensitivity and uncertainty analysis for parameterization of multiphase flow models. *Transport in Porous Media*, *140*(1), 27-57.
12. Bourbiaux, B. J., & Kalaydjian, F. J. (1990). Experimental study of cocurrent and countercurrent flows in natural porous media. *SPE Reservoir Engineering*, *5*(03), 361-368.
13. Brooks, R.H. and Corey, A.T. (1964). Hydraulic Properties of Porous Media. Hydrology Papers, No. 3, Colorado State U., Fort Collins, Colorado.
14. Chen, A. L., & Wood, A. C. (2001, September). Rate effects on water-oil relative permeability. In *Proceedings of the International Symposium of the Society of Core Analysts, Edinburgh, Scotland* (pp. 17-19).
15. Cheng, Y. C., Di, Q. F., Gu, C. Y., Ye, F., Hua, S., & Yang, P. Q. (2015). Visualization study on fluid distribution and end effects in core flow experiments with low-field mri method. *Journal of hydrodynamics*, *27*(2), 187-194.
16. Dullien, F. A. (1992). *Porous media: fluid transport and pore structure, 2nd Ed*. Academic press, San Diego, California.
17. Gupta, R., & Maloney, D. R. (2016). Intercept method—A novel technique to correct steady-state relative permeability data for capillary end effects. *SPE Reservoir Evaluation & Engineering*, *19*(02), 316-330.
18. Henderson, G. D., Danesh, A., Tehrani, D. H., Al-Shaidi, S., & Peden, J. M. (1998). Measurement and correlation of gas condensate relative permeability by the steady-state method. *SPE Reservoir Evaluation & Engineering*, *1*(02), 134-140.
19. Hove, A. O., Ringen, J. K., & Read, P. A. (1987). Visualization of laboratory corefloods with the aid of computerized tomography of X-rays. *SPE Reservoir Engineering*, *2*(02), 148-154.
20. Huang, D. D., & Honarpour, M. M. (1998). Capillary end effects in coreflood calculations. *Journal of Petroleum Science and Engineering*, *19*(1-2), 103-117.

21. Jeong, G. S., Ki, S., Lee, D. S., & Jang, I. (2021). Effect of the Flow Rate on the Relative Permeability Curve in the CO2 and Brine System for CO2 Sequestration. *Sustainability*, *13*(3), 1543.
22. Lenormand, R., Lorentzen, K., Maas, J. G., & Ruth, D. (2017). Comparison of four numerical simulators for SCAL experiments. *Petrophysics-The SPWLA Journal of Formation Evaluation and Reservoir Description*, *58*(01), 48-56.
23. Leverett, M. (1941). Capillary behavior in porous solids. *Transactions of the AIME*, *142*(01), 152-169.
24. Maas, J. G., & Schulte, A. M. (1997, September). Computer simulation of Special Core Analysis (SCAL) flow experiments shared on the Internet. In *SCA-9719 presented at the SCA 1997 conference, Calgary, Canada* (Vol. 10, p. 92).
25. McPhee, C., Reed, J. and Zubizarreta, I. (2015). Best practice in coring and core analysis. In Developments in Petroleum Science, 1–15.
26. Moghaddam, R. N. & Jamiolahmady, M. (2019) Steady State Relative Permeability Measurements of Tight and Shale Rocks Considering Capillary End Effect. *Transport in Porous Media*, *128*, 75-96.
27. Li Y., Wang, S., Kang, Z., Yuan, Q., Xue, X., Yu, C. & Zhang, X. (2021). Research on the Correction Method of the Capillary End Effect of the Relative Permeability Curve of the Steady State. *Energies*, *14*, 4528.
28. Odeh, A. S., & Dotson, B. J. (1985). A method for reducing the rate effect on oil and water relative permeabilities calculated from dynamic displacement data. *Journal of petroleum technology*, *37*(11), 2-051.
29. Osoba, J. S., Richardson, J. G., Kerver, J. K., Hafford, J. A., & Blair, P. M. (1951). Laboratory measurements of relative permeability. *Journal of Petroleum Technology*, *3*(02), 47-56.
30. Rapoport, L. A., & Leas, W. J. (1953). Properties of linear waterfloods. *Journal of Petroleum Technology*, *5*(05), 139-148.
31. Reed, J., & Maas, J. (2018, August). Review of the intercept method for relative permeability correction using a variety of case study data. In *The International Symposium of the Society of Core Analysts*.
32. Richardson, J. G., Kerver, J. K., Hafford, J. A., & Osoba, J. S. (1952). Laboratory determination of relative permeability. *Journal of Petroleum Technology*, *4*(08), 187-196.

33. Valdez, A. R., Rocha, B. M., Chapiro, G., & dos Santos, R. W. (2020). Uncertainty quantification and sensitivity analysis for relative permeability models of two-phase flow in porous media. *Journal of Petroleum Science and Engineering*, *192*, 107297.
34. Virnovsky, G. A., Guo, Y. & Skjæveland, S. M. (1995, May). Relative permeability and capillary pressure concurrently determined from steady-state flow experiments. In *IOR 1995-8th European Symposium on Improved Oil Recovery* (pp. cp-107). European Association of Geoscientists & Engineers.
35. Virnovsky, G. A., Vatne, K. O., Skjaeveland, S. M., & Lohne, A. (1998, September). Implementation of multirate technique to measure relative permeabilities accounting. In *SPE Annual Technical Conference and Exhibition*. OnePetro.
36. Wellington, S. L., & Vinegar, H. J. (1987). X-ray computerized tomography. *Journal of petroleum technology*, *39*(08), 885-898.
37. Yeganeh, M., Hegner, J., Lewandowski, E., Mohan, A., Lake, L. W., Cherney, D., ... & Jaishankar, A. (2016, April). Capillary desaturation curve fundamentals. In *SPE Improved Oil Recovery Conference*. OnePetro.
38. Zou, S., Liu, Y., Cai, J., & Armstrong, R. T. (2020). Influence of capillarity on relative permeability in fractional flows. *Water Resources Research*, *56*(11), e2020WR027624.

Nomenclature

Roman

F	=	Injected water fraction, -
f_w	=	Water fractional flow function, -
J	=	Scaled capillary pressure, -
k_{ri}	=	Phase relative permeability, -
K	=	Absolute permeability, m^2
k_i^*	=	Relative permeability end point, -
L	=	Core length, m
N_0	=	Capillary number, -
p_i	=	Phase pressure, Pa
P_c	=	Capillary pressure, Pa
s_i	=	Phase saturation, -
S_i	=	Normalized phase saturation, -
S_1	=	Normalized water saturation at the inlet ($Y = 1$), -
S_{eq}	=	Normalized water saturation at which capillary pressure is zero, -
S_r	=	Normalized reference water saturation (obtained with no end effects), -
$\bar{S}$	=	Average normalized saturation in the core, -
$\bar{S}^*$	=	Average normalized saturation in end effect region, -
$\bar{s}_w^*$	=	Average saturation in end effect region, -
u_i	=	Darcy phase velocity, m / s

v_i	=	Interstitial velocity, m / s
Y	=	Scaled distance from outlet, -

Greek

ϕ	=	Porosity, -
μ_i	=	Phase viscosity, Pa s
σ_{ow}	=	Interfacial tension, N / m
λ_i	=	Phase mobility, 1 / (Pa s)
Δp_i	=	Phase pressure drop, Pa
Δp_I	=	Constant pressure drop from end effects at high rates, Pa
Δp_{ref}	=	Pressure drop without end effects, Pa

Indices

*	=	Evaluated based on the saturation S^*
eq	=	Zero capillary pressure condition
i	=	Phase index
nw	=	Non-wetting phase (can be water or oil)
o	=	Oil
r	=	Reference (no end effects)
T	=	Total
w	=	Water